Optical conductivity of warm dense matter within a wide frequency range using quantum statistical and kinetic approaches

M. Veysman,[1,*] G. Röpke,[2,3,†] M. Winkel,[4,5] and H. Reinholz[2,6,‡]

[1]*Joint Institute for High Temperatures (JIHT) RAS, Izhorskaya 13/19, Moscow 125412, Russia*

[2]*Universität Rostock, Institut für Physik, 18051 Rostock, Germany*

[3]*National Research Nuclear University (MEPhI), 115409 Moscow, Russia*

[4]*Institute for Advanced Simulation, Juelich Supercomputing Centre, Forschungszentrum, Juelich GmbH, 52425 Juelich, Germany*

[5]*ExtreMe Matter Institute EMMI, GSI Helmholtzzentrum fuer Schwerionenforschung GmbH, Planckstrasse 1, 64291 Darmstadt, Germany*

[6]*The University of Western Australia, School of Physics, Crawley, Western Australia 6009, Australia*

(Received 2 February 2016; published 18 July 2016)

Fundamental properties of warm dense matter are described by the dielectric function, which gives access to the frequency-dependent electrical conductivity; absorption, emission, and scattering of radiation; charged particles stopping; and further macroscopic properties. Different approaches to the dielectric function and the related dynamical collision frequency are compared in a wide frequency range. The high-frequency limit describing inverse bremsstrahlung and the low-frequency limit of the dc conductivity are considered. Sum rules and Kramers-Kronig relation are checked for the generalized linear response theory and the standard approach following kinetic theory. The results are discussed in application to aluminum, xenon, and argon plasmas.

DOI: 10.1103/PhysRevE.94.013203

I. INTRODUCTION

Interaction of laser radiation with matter is utilized for many modern applications, like creation of sources of high-energy particles and short-wavelength radiation [1–5]. Under irradiation of solid targets with intense laser pulses, matter undergoes transformations from a cold solid up to hot and dense plasma (warm dense matter, WDM) and further to weakly coupled plasmas with properties rapidly varying in time and space. Therefore, for a correct description of laser-matter interaction in very different regions of parameter values for mass density and electron and ion temperatures, one needs wide-range models for the optical properties of WDM, which are determined by the permittivity or dielectric function (DF) $\varepsilon(\boldsymbol{k},\omega)$.

Knowing wide-range expressions for $\varepsilon(\boldsymbol{k},\omega)$ and also transport coefficients and equations of state, one can determine space and time dependencies of laser-heated matter by means of hydrodynamic codes such as LASNEX [6], MEDUSA [7], MULTI-FS [8], or the code of the JIHT group [9–12]. Primarily, those codes use semiempirical models for $\varepsilon(\boldsymbol{k},\omega)$ and a corresponding effective electron-ion (electron-phonon) collision frequency [9,13], which are derived from kinetic equations and give known limits for the case of weakly coupled plasmas and handbook values for cold solids and are based on physically reasonable estimates and experimental data in the intermediate region [8–10]. The elaboration of a systematic many-particle approach that covers distinct regions like cold metals and hot strongly coupled plasmas is a challenging problem in nonequilibrium statistical physics.

Besides this, the advantage of such an approach is the description of laser interaction with matter for a wider range of laser parameters, from infrared to x-ray wavelengths. This is requested keeping in mind recent achievements in the construction of powerful laser systems operating with ultraviolet and x-ray wavelengths [14–16]. Note that local thermodynamic equilibrium in WDM is established on the fs scale after the excitation by laser irradiation (see, e.g., [17]) and is assumed for the following considerations.

The most strict many-particle approach for calculating the permittivity of WDM consists of a quantum statistical (QS) description of the reaction of the system to external perturbations; see [18] (often also called the "Zubarev approach"). Within the QS approach, both fundamental theoretical approaches can be derived, as demonstrated in a recent paper [19]: The linear response theory (LRT) [20,21] follows from the QS formalism if one chooses moments of the particle distribution function as relevant observables, and the kinetic approach follows if density fluctuations are chosen as sets of relevant observables. In turn, the kinetic approach can be realized on the basis of quantum kinetic equations [22], or, alternatively, using classical kinetic theory (KT) [23] and the concept of cross sections, which leads to the formulation of kinetic equations with Boltzmann or Fokker-Planck collision integrals. In the most simple form, when one can disregard electron-electron collisions, the electron-ion collision integral can be written in relaxation time approximation, which leads to simple expressions for the permittivity, which are widely used in hydrodynamic codes [8,12,24,25].

Another approach using a classical method of moments which satisfies the sum rules [26] is a promising alternative to derive analytical approximations but will not be further considered here.

Following LRT, transport coefficients and expressions for inverse bremsstrahlung absorption are expressed by equilibrium correlation functions which can be calculated with the help of the Green's functions technique in a systematic way. This procedure takes consistently into account many-particle effects, such as electron and ion correlations and dynamical screening, and also effects of strong collisions relevant for large-angle scattering [20,27]. An account of these effects can

*bme@ihed.ras.ru

†gerd.roepke@uni-rostock.de

‡heidi.reinholz@uni-rostock.de

be essential for studies of optical properties of WDM, i.e., at temperatures of the order of $T \sim 0.1$–10^2 eV and densities up to the order of solid ones [17]. An alternative to the perturbative treatment using Green's functions leading to analytical expressions is the direct evaluation of the equilibrium correlation functions using molecular dynamics (MD) simulations of ions combined with the density functional theory (DFT) for the electrons as denoted by the Kubo-Greenwood approach; see [28–31]. The reliability of results obtained by means of perturbative (using Green's functions) approaches was confirmed recently by comparison with numerical MD simulations [28,32,33].

A consistent treatment of strong-coupling effects and the frequency dependence of the dynamical conductivity [19,27] are the strength of the LRT approach. On the other hand, the respective expressions can be rather cumbersome and therefore difficult for implementation in hydrodynamic codes. This is why the elaboration of approximate semiempirical formulas and interpolation models is of great interest, especially keeping in mind the necessity to make connection with experimental data and MD simulations in the region of WDM parameters, where one cannot extract small parameters for the theory to be built.

The principal ideas of the LRT approach are summarized in Sec. II. In particular, a generalized screening parameter taking into account dynamical screening effects is proposed. The KT following the solution of the Fokker-Planck equations is described in Sec. III. Results are discussed in Sec. IV. A comparison will be made between calculations of the DF using LRT, with results obtained from the semiempirical model [9,10,13] based on KT and with other models utilizing the concept of relaxation time approximation and Coulomb logarithm [34,35]. In addition, calculations of an effective frequency for electron-ion collisions on the basis of quantum [19] and classical [23] kinetic equations are compared. A brief description of the models compared with each other as well as used for the comparison with experimental data is given in Sec. IV A. The influence of plasma inhomogeneities and interband transitions is discussed in Sec. V and investigated considering the reflectivity of shock compressed plasmas.

II. DIELECTRIC FUNCTION FROM QUANTUM STATISTICAL APPROACH USING LRT

Warm dense matter can be described as a system of interacting particles, electrons, and ions. In contrast to a first principles approach that treats the electrons and atomic nuclei as constituents, we consider a chemical picture where we have ions (localized electrons bound to nuclei) and free electrons (unbound electrons in itinerant states, extending over the entire volume), with free electron density n and temperature T. We use energy units, thus setting $k_B = 1$. In general, there are ions with different ionization and excitation stages. For simplicity, we consider the ion components in terms of an average ion charge Z with the particle density $n_\mathrm{i} = n/Z$ due to charge neutrality. The ion temperature is denoted as T_i. The cgs system of units is used in the following, thus replacing $e^2/(4\pi\epsilon_0)$ in previous papers (e.g., Refs. [19,27]) with e^2. Note that at high densities quasiparticles can be introduced, approximating the mean-field effects by a self-energy shift and an effective mass. In condensed matter, the electrons in itinerant states are given by the conduction band, whereas the valence band electrons are bound to the ions.

The ions are treated in adiabatic approximation [36] via the static ion structure factor, $S_\mathrm{ii}(\boldsymbol{k}) = n_\mathrm{i}^{-1}\sum_{i,j}\langle\exp[i\boldsymbol{k}\cdot(\boldsymbol{R}_i - \boldsymbol{R}_j)]\rangle$, which describes static correlations of ions at positions $\boldsymbol{R}_j$ such as lattice formation (ions in a unit volume are considered; brackets $\langle\cdots\rangle$ denote statistical average).

In the liquid phase, the ion structure factor also has to be considered. For the interaction of electrons with collective excitations of the ion lattice, i.e., phonons, one should consider time-dependent positions $\boldsymbol{R}_j(t)$ leading to the dynamical ionic structure factor $S_\mathrm{ii}(\boldsymbol{k},\omega) = n_\mathrm{i}^{-1}\sum_{i,j}\int dt\,\exp[-i\omega t]\langle\exp[i\boldsymbol{k}\cdot(\boldsymbol{R}_i(t) - \boldsymbol{R}_j)]\rangle$.

In the following derivation within LRT and KT, the static structure factor is taken to be $S_\mathrm{ii}(\boldsymbol{k}) = 1$ for simplicity (noncorrelated ions). The influence of ion correlations is considered later in Secs. II G and IV.

We express the DF in terms of equilibrium correlation functions. For the Hamiltonian of the electron-ion system we consider the electronic degrees of freedom only,

$$H = \sum_p E_p \hat{a}_p^\dagger \hat{a}_p + \sum_{pk} V_\mathrm{ei}(k)\hat{a}_{p+k}^\dagger \hat{a}_p + \frac{1}{2}\sum_{p_1 p_2 k} V_\mathrm{ee}(k)\hat{a}_{p_1+k}^\dagger \hat{a}_{p_2-k}^\dagger \hat{a}_{p_2}\hat{a}_{p_1}\,. \tag{1}$$

with $E_p = \hbar^2 p^2/(2m)$. Interactions between ions and electrons $V_\mathrm{ei}(k) = V(k)$ are given by the Coulomb potential $V(k) = -Zv(k)$ and $V_\mathrm{ee}(k) = v(k) = 4\pi e^2/k^2$ is the potential of the e-e interaction.

Note that in the general case pseudopotentials $V_\mathrm{ei}^\mathrm{ps}(k)$ may have to be considered. They reflect the fact that the fundamental Coulomb interaction between charged particles is modified if we introduce quasiparticles such as band electrons in the lattice formed by ions. Besides this, the structure of complex ions can also influence their interaction with free electrons via interaction of bound and free electrons. This is discussed in Secs. II G and IV at a phenomenological level. In expressions given below for the Born approximation, we have to replace

$$|V_\mathrm{ei}(\boldsymbol{k})|^2 = \left|V_\mathrm{ei}^\mathrm{ps}(k)\right|^2 S_\mathrm{ii}(\boldsymbol{k}). \tag{2}$$

Generally speaking, time variation of the current density contains intraband and interband contributions. Consequently, the response of the system is determined by intraband (single band, sb) as well as interband (bound-bound, bb) scattering mechanisms. Below we restrict ourselves to intraband contributions which are described by a plasma model for WDM. The interband contribution to the DF is considered in Sec. V B at a more phenomenological level.

In the present treatment we disregard electron-phonon interactions and umklapp processes, which is valid at temperatures sufficiently higher than melting temperatures. Also, temperatures are considered such that the plasma coupling parameter $\Gamma_\mathrm{ei} = Ze^2/(R_0 T) \lesssim 1$, where

$$R_0 = (4\pi n_\mathrm{i}/3)^{-1/3} \tag{3}$$

is the Wigner-Seitz radius. The degeneracy parameter $\Theta = \epsilon_F^{-1} = T/E_F = 2mT/\hbar^2(3\pi^2 n)^{-2/3}$, where E_F is the Fermi energy, can be arbitrary, if it is not stated otherwise.

Before proceeding further, common expressions for the DF and its relation to the polarization and response functions are considered briefly.

A. General expressions for the contribution of electrons to the DF

In accordance with common theory [37], the permittivity of an isotropic medium is expressed as $\varepsilon_{ij}(\boldsymbol{k},\omega) = (\delta_{ij} - k_i k_j/k^2)\varepsilon_\perp(\mathbf{k},\omega) + k_i k_j/k^2 \varepsilon_\parallel(\boldsymbol{k},\omega)$, where $\varepsilon_\parallel$, $\varepsilon_\perp$, ω, and $\boldsymbol{k}$ are longitudinal and transverse parts of permittivity, frequency of radiation, and wave vector, respectively. $k = |\boldsymbol{k}|$; indexes i, j denote respective components. From Maxwell equations, keeping in mind the electric field of polarization charge and density fluctuations, one can find equivalent expressions for the longitudinal permittivity ε [18,38] (here and below, index "$\parallel$" is omitted for brevity),

$$\varepsilon(\boldsymbol{k},\omega) = 1 - v(k)\Pi(\boldsymbol{k},\omega) = [1 + v(k)\chi(\boldsymbol{k},\omega)]^{-1}, \quad (4)$$

where $\Pi(\boldsymbol{k},\omega) = \rho(\boldsymbol{k},\omega)/\phi_{\rm tot}(\boldsymbol{k},\omega)$ is the polarization function and $\chi(\boldsymbol{k},\omega) = \rho(\boldsymbol{k},\omega)/\phi_{\rm ext}(\boldsymbol{k},\omega)$ is the response function. $\phi_{\rm tot} = \phi_{\rm pol} + \phi_{\rm ext}$ is the total scalar potential consisting of the external potential $\phi_{\rm ext}$ and the potential of polarization charge $\phi_{\rm pol}$, $\rho(\boldsymbol{k},\omega)$ is the Fourier transform of the quantum-mechanical average of density fluctuations, $\rho(\boldsymbol{k},t) = \langle\Psi(t)|\rho_{\boldsymbol{k}}|\Psi(t)\rangle$, where $\rho_{\boldsymbol{k}} = \sum_l \int d^3r \delta(\boldsymbol{r} - \boldsymbol{r}_l) e^{-i\boldsymbol{k}\boldsymbol{r}} = \sum_l e^{-i\boldsymbol{k}\boldsymbol{r}_l}$ is the Fourier component of the charge particle density and $\Psi(t)$ the full wave function of the system. According to Eq. (4), the function $\chi(\boldsymbol{k},\omega)$ is connected to the polarization function $\Pi(\boldsymbol{k},\omega)$ by the relation

$$\Pi(\boldsymbol{k},\omega) = \chi(\boldsymbol{k},\omega)/[1 + v(k)\chi(\boldsymbol{k},\omega)]. \quad (5)$$

The response function determines the reaction of the system on external perturbations.

At zeroth order of interaction, the permittivity is determined by the polarization function in random phase approximation (RPA) [18,38,39],

$$\Pi_{\rm RPA}(\boldsymbol{k},\omega) = \chi_0(\boldsymbol{k},\omega) = 2\sum_{\boldsymbol{p}} \frac{f_{\boldsymbol{p}+\boldsymbol{k}} - f_{\boldsymbol{p}}}{E_{\boldsymbol{p}+\boldsymbol{k}} - E_{\boldsymbol{p}} - (\hbar\omega + i\delta)}, \quad (6)$$

where spin summation gives the factor 2, $f_{\boldsymbol{p}} = f_p = [1 + e^{(E_p - \mu)/T}]^{-1}$ is the electron distribution function, μ is the chemical potential of the electrons, and the limit $\delta \to +0$ is considered.

If the interaction between the charged particles is taken into account, the local microscopic field acting on an electron differs from the average macroscopic field. In this case the polarization of the electron gas is different from the sum of the polarization of its individual particles [39] and the RPA polarization function (6) is replaced with

$$\Pi(\boldsymbol{k},\omega) = \frac{\Pi_{\rm RPA}(\boldsymbol{k},\omega)}{1 + G(\boldsymbol{k},\omega)\Pi_{\rm RPA}(\boldsymbol{k},\omega)v(k)}, \quad (7)$$

where $G(\boldsymbol{k},\omega)$ is the *local field factor* [27,39,40], which contains all effects due to charged particle interactions, in particular, dynamical screening, correlations, and strong collisions.

B. Response function and local field factor in terms of correlation functions

Using the method of quantum statistical operator [18], within LRT one can show [21,27,41] that the response function is

$$\chi^{-1}(\boldsymbol{k},\omega) = -i\omega T M(\boldsymbol{k},\omega)/k^2, \quad (8)$$

where

$$M(\boldsymbol{k},\omega) = \begin{vmatrix} 0 & \boldsymbol{M}_N \\ \check{\boldsymbol{M}}_N & \boldsymbol{M}_{NN} \end{vmatrix}^{-1} |\boldsymbol{M}_{NN}|, \quad (9)$$

$\boldsymbol{M}_N$ is the row of elements $\{M_1, \ldots, M_N\}$, $\check{\boldsymbol{M}}_N$ is the column of elements $\{\check{M}_1, \ldots, \check{M}_N\}$, and $\boldsymbol{M}_{NN}$ is the matrix of elements $\{M_{ij}\}$, $i, j = 1, \ldots, N$, where

$$\begin{aligned} M_n(\boldsymbol{k},\omega) &= (\boldsymbol{B}_n(\boldsymbol{k},\omega); \boldsymbol{J}_{\boldsymbol{k}}), \\ \check{M}_n(\boldsymbol{k},\omega) &= (\boldsymbol{J}_{\boldsymbol{k}}; \boldsymbol{B}_n(\boldsymbol{k},\omega)), \\ M_{mn}(\boldsymbol{k},\omega) &= (\boldsymbol{B}_m; [\dot{\boldsymbol{B}}_n + i\omega\boldsymbol{B}_n]) \\ &\quad + \left\langle \left[\dot{\boldsymbol{B}}_m - \frac{\langle \dot{\boldsymbol{B}}_m; \boldsymbol{J}_{\boldsymbol{k}}\rangle_{\omega+i\delta}}{\langle \boldsymbol{B}_m; \boldsymbol{J}_{\boldsymbol{k}}\rangle_{\omega+i\delta}} \boldsymbol{J}_{\boldsymbol{k}}\right]; [\dot{\boldsymbol{B}}_n + i\omega\boldsymbol{B}_n] \right\rangle_{\omega+i\delta}. \end{aligned} \quad (10)$$

Here $\boldsymbol{J}_{\boldsymbol{k}} = e/m \sum_{\boldsymbol{p}} \hbar\boldsymbol{p}\, n_{\boldsymbol{p},\boldsymbol{k}}$ is the operator of the current density, $n_{\boldsymbol{p},\boldsymbol{k}} = a^+_{\boldsymbol{p}-\boldsymbol{k}/2} a_{\boldsymbol{p}+\boldsymbol{k}/2}$ is the Wigner form of the single-particle density matrix in the momentum representation, and $\{\boldsymbol{B}_n\}$, $n = 1, \ldots, N$, is the chosen set of observables in the form of moments of the density matrix

$$\boldsymbol{B}_n(\boldsymbol{k}) = \boldsymbol{P}_{\boldsymbol{k},n} = \sum_{\boldsymbol{p}} \hbar\boldsymbol{p}(E_p/T)^{(n-1)/2} n_{\boldsymbol{p},\boldsymbol{k}}, \quad (11)$$

where $\boldsymbol{J}_{\boldsymbol{k}} = e\boldsymbol{P}_{\boldsymbol{k},0}/m$. In (10), the expressions like

$$(\hat{A}; \hat{B}) = \int_0^\beta d\tau\, {\rm Tr}\{\hat{A}(-i\hbar\tau)\hat{B}^+\rho_0\} \quad (12)$$

denote Kubo scalar products of operators $\hat{A}$ and $\hat{B}$, where the operator $\hat{A}$ is taken in Heisenberg representation $\hat{A}(t) = e^{i\hat{H}t/\hbar}\hat{A}e^{-i\hat{H}t}$, where $\rho_0 = {\rm Z}^{-1}\exp[-(\hat{H} - \mu\hat{N})/T]$ is the equilibrium statistical operator of the grand-canonical ensemble with ${\rm Z} = {\rm Tr}\{e^{-(\hat{H}-\mu\hat{N})/T}\}$, where $\hat{N}$ is the electron particle number operator. The equilibrium correlation function

$$\langle\hat{A}; \hat{B}\rangle_z = \int_0^\infty dt e^{izt}(\hat{A}(t); \hat{B}) \quad (13)$$

denotes the Laplace transform of the Kubo scalar product of the operators.

From Eqs. (4), (7), and (8) one can express the local field factor in terms of correlation functions (10) containing the

observables B_n as

$$G(\boldsymbol{k},\omega) = 1 + \frac{1}{v(k)}\left[\frac{1}{\chi(\boldsymbol{k},\omega)} - \frac{1}{\chi_0(\boldsymbol{k},\omega)}\right] = -i\omega T M(\boldsymbol{k},\omega) + 1 - [v(k)\chi_0(\boldsymbol{k},\omega)]^{-1}, \quad (14)$$

where $\chi_0(\boldsymbol{k}\omega)$ and $M(\boldsymbol{k},\omega)$ are given by Eqs. (6) and (9), respectively.

C. Long-wavelength limit and dynamical collision frequency

In the following it is assumed that the mean free path of an electron between successive collisions $V_{\rm th}/\nu_{\rm eff}$ and the path during the laser period $V_{\rm th}/\omega$ are much smaller than the characteristic length scale of the electric-field nonuniformity L_∇. Here $V_{\rm th} = \sqrt{T/m}$ is proportional to the mean thermal velocity and $\nu_{\rm eff}$ is the characteristic collision frequency of electrons; see below Sec. III. L_∇ can be of the order of the plasma skin depth $l_s = c/\omega_{\rm pl}$, which is created on the surface of a solid target if irradiated by short (subpicosecond) laser pulses, where $\omega_{\rm pl}^2 = 4\pi e^2 n/m$ is the plasma frequency [42]. In this case, one can disregard the spacial dispersion of the plasma and calculate its optical properties within the *long-wavelength limit*, i.e., for $k \to 0$. For warm dense matter, the above inequalities mean that the considered long-wavelength limit for uniform plasmas is valid for electron temperatures below several hundred eV [24].

In the long-wavelength limit is $\lim_{k\to 0} v(k)\Pi_{\rm RPA} = \omega_{\rm pl}^2/\omega^2$. Using Eqs. (4) and (7), one finds a Drude-like expression for the permittivity,

$$\lim_{k\to 0} \varepsilon(\boldsymbol{k},\omega) = \varepsilon(\omega) = 1 - \frac{\omega_{\rm pl}^2}{\omega[\omega + i\nu(\omega)]}, \quad (15)$$

where the dynamical collision frequency,

$$\nu(\omega) = -\frac{\omega_{\rm pl}^2}{i\omega}\lim_{k\to 0} G(\boldsymbol{k},\omega) \quad (16)$$

$$= \omega_{\rm pl}^2 T M(0,\omega) + i\left(\omega - \omega_{\rm pl}^2/\omega\right), \quad (17)$$

is, generally speaking, a complex quantity which is closely related to the effective collision frequency of electrons (see below).

It should be noted that in the long-wavelength limit there is no difference between longitudinal and transverse permittivities, and expression (15), originally derived for the longitudinal permittivity, is also valid for the transverse one.

In accordance with Eqs. (17), (9), and (10), the dynamical collision frequency $\nu(\omega)$ is expressed in terms of correlation functions. The respective expressions can be derived directly from the general expressions (10), as done in Refs. [19,27]. It is instructive to describe briefly the derivation directly from linear response equations; see Appendix A. Subsequently, the permittivity (15) can be calculated using the dynamical collision frequency

$$\nu(\omega) = \nu_1(\omega) r_\omega(\omega), \quad (18)$$

$$\nu_1(\omega) = \omega_{\rm au}\frac{\mathfrak{C}_{11}}{\mathfrak{N}_{11}}, \quad r_\omega(\omega) = \frac{\mathfrak{N}_{11}}{\mathfrak{C}_{11}}\frac{1 + i\omega^*\sum_m \mathfrak{N}_{1m}\mathcal{F}_m}{\sum_m \mathfrak{N}_{1m}\mathcal{F}_m} \quad (19)$$

(for details and elimination of $\mathcal{F}_m$ see Appendix B), with the following designation of dimensionless correlation functions and response parameter

$$\mathfrak{N}_{nm} = \frac{(\hat{\boldsymbol{P}}_n;\hat{\boldsymbol{P}}_m)}{mnT}, \quad \mathfrak{C}_{nm}(\omega) = \frac{\langle\hat{\boldsymbol{P}}_n;\hat{\boldsymbol{P}}_m\rangle_{\omega+i\delta}}{mnT\omega_{\rm au}}, \quad F_m = \mathcal{F}_m\frac{e\boldsymbol{E}}{mT}, \quad (20)$$

where $\omega_{\rm au}$ is the atomic unit of frequency, $\hbar\omega_{\rm au} = E_H = me^4/\hbar^2 \approx 27.2$ eV is Hartree energy, and $\omega^* = \omega/\omega_{\rm au}$ is the dimensionless frequency.

In Eq. (18), $\nu_1(\omega)$ is the collision frequency calculated in the one-moment approximation. For this, only one observable $\hat{\boldsymbol{B}}_1 = \hat{\boldsymbol{P}}_1$ is used in (A3). In order to take into account higher moments of the distribution function [see Eq. (11)], the so called renormalization factor $r_\omega(\omega)$ is introduced [19,27]. A low-order expansion of the correlation functions within perturbation theory with respect to the interaction parameter e^2 may lead to different results if different *reduced* sets of relevant observables are used. Therefore, partial summation of the perturbation expansion must be performed to obtain correct results for transport coefficients in this case; see [43] and references therein.

Equations (18) and (19) determine implicitly an effective collision frequency of electrons in terms of dimensionless correlation functions $\mathfrak{C}_{nm}$ through dimensionless response parameters $\mathcal{F}_n$, which are solutions of the system of Eqs. (A8). In previous works (see, for example, [19,27]) correlation functions with only first and third moments of the distribution function (11) in the sum (19) were considered. It was shown that this leads to an accuracy of few % for the calculation of the renormalization factor, at least at low frequencies ($\omega/\omega_{\rm pl} < 1$), as well as at high frequencies $\omega > \omega_{\rm pl}$, when $\lim_{\omega\to\infty} r_\omega(\omega) \to 1$. Using these two moments, the solution of (A8) makes it possible to write down a clearly structured expression for $r_\omega(\omega)$ in terms of those correlation functions:

$$r_\omega(\omega) = \frac{1}{\mathfrak{C}_{11}}\frac{1 + i\omega^* Q_\omega}{Q_\omega}, \quad Q_\omega = \frac{\mathfrak{A}_{33} - 2\mathfrak{N}_{31}\mathfrak{A}_{31} + \mathfrak{N}_{31}^2\mathfrak{A}_{11}}{\mathfrak{A}_{11}\mathfrak{A}_{33} - \mathfrak{A}_{31}^2}, \quad \mathfrak{A}_{lm} = \mathfrak{C}_{lm} - i\omega^*\mathfrak{N}_{lm}, \quad l,m \geqslant 1. \quad (21)$$

For the calculation of the correlation functions $\mathfrak{N}_{lm}$, $l,m \geqslant 1$, the following expressions are used (see Ref. [28]),

$$\mathfrak{N}_{lm} = \frac{\Gamma[(l+m+3)/2]}{\Gamma(5/2)}\frac{I_{(l+m-1)/2}(\epsilon_\mu)}{I_{1/2}(\epsilon_\mu)}, \quad l,m \geqslant 1, \quad (22)$$

with $\epsilon_\mu = \mu/T$, from which one has $\mathfrak{N}_{11} = 1$ and

$$\mathfrak{N}_{31} = \frac{5}{2}\frac{I_{3/2}(\epsilon_\mu)}{I_{1/2}(\epsilon_\mu)}, \quad \mathfrak{N}_{33} = \frac{35}{4}\frac{I_{5/2}(\epsilon_\mu)}{I_{1/2}(\epsilon_\mu)}. \quad (23)$$

Here $I_\nu(y) = \Gamma(\nu+1)\int_0^\infty x^\nu[e^{x-y}+1]^{-1}dx$ are Fermi integrals; the dimensionless chemical potential is expressed via the inverse Fermi integral $X_{1/2}(x)$ reverse to the Fermi integral $I_{1/2}(x)$ as

$$\epsilon_\mu = X_{1/2}\left(2\epsilon_{\rm F}^{3/2}/3\right). \quad (24)$$

In the nondegenerate case $I_\nu(\epsilon_\mu) = e^{\epsilon_\mu}$ for all ν and $\mathfrak{N}_{31} = 5/2$, $\mathfrak{N}_{33} = 35/4$; see Ref. [19].

According to the definitions (13) and (20), the correlation functions $\mathfrak{C}_{nm}(\omega)$ are expressed in terms of correlation functions of occupation numbers as

$$\mathfrak{C}_{nm}(\omega) = \frac{\beta\hbar^2}{mn\omega_{\rm au}} \sum_{p,p'} p_z p'_z (\beta E_p)^{\frac{n+1}{2}} (\beta E_{p'})^{\frac{m+1}{2}} \times \langle \hat{n_p}; \hat{n_{p'}} \rangle_{\omega+i\delta}, \tag{25}$$

where $\hat{n}_p = \hat{n}_{p,k=0}$. Using the time dependence $\dot{\hat{n_p}} = (i/\hbar)[\hat{H},\hat{n}_p]$, the Hamiltonian (1), and the relation $\langle \hat{A}; \hat{B} \rangle_z = \frac{i}{\beta}\int_{-\infty}^{\infty} \frac{d\omega'}{\pi} \frac{{\rm Im}\{\mathcal{G}_{AB^\dagger}\}(\omega'+i\delta)}{\omega'(z-\omega')}$, where $\mathcal{G}_{AB^\dagger}$ is the thermodynamic Green's function, one can express correlation functions $\mathfrak{C}_{nm}$ in terms of four-particle Green's functions, containing products of potentials for electron-ion $V_{\rm ei}(q)V_{\rm ei}(q')$ or electron-electron $V_{\rm ee}(q)V_{\rm ee}(q')$ interactions; see, for example, [27].

These Green's functions can be evaluated by diagram technique. At the lowest order of interaction the four-particle Green's functions are expressed as products of single-particle Green's functions and the Born approximation follows. Summation of ring diagrams leads to account for dynamical screening of interaction potential and permits one to avoid artificial cutoffs as adopted in classical KT. Summation of ladder diagrams permits one to account for strong collisions with large-angle scattering; see Ref. [27] for details. It should be noted that for simplicity it is reasonable to calculate the renormalization factor (19) in the Born or screened Born (see below) approximation and take into account strong-coupling effects only in the calculation of the collision frequency $\nu_1(\omega)$ in a one-moment approximation while calculating the correlation function $\mathfrak{C}_{11}(\omega)$.

The account of screening of the interaction potential is necessary to avoid divergences at low frequencies [43] and to get numerically accurate results at finite frequencies. An account of the dynamical screening via summation of ring diagrams [20,27] gives rise to the Lenard-Balescu result for the dynamical collision frequency $\nu_1(\omega)$. Adopting the dimensionless units

$$\tilde{k} = k\lambda\!\!\!^{-} = k\hbar/\sqrt{mT}; \quad \tilde{\omega} = \hbar\omega/T, \tag{26}$$

it can be written in the form

$$\tilde{\nu}^{\rm LB}(\tilde{\omega}) = \frac{i\nu_0 Z}{\tilde{\omega}} \int_0^\infty \tilde{k}^2 d\tilde{k} \left[\varepsilon^{-1}_{\rm RPA}(\tilde{k},\tilde{\omega}) - \varepsilon^{-1}_{\rm RPA}(\tilde{k},0)\right], \tag{27}$$

with $\nu_0 = 2\sqrt{\hbar\omega_{\rm au}/T}/(3\pi)$ and $\varepsilon_{\rm RPA} = \varepsilon'_{\rm RPA} + i\varepsilon''_{\rm RPA}$ is the RPA permittivity,

$$\varepsilon'_{\rm RPA}(\tilde{k},\tilde{\omega}) = 1 + \frac{\nu_0}{\tilde{k}^3}\left[g\left(\frac{\tilde{\omega}}{\tilde{k}} + \frac{\tilde{k}}{2}\right) - g\left(\frac{\tilde{\omega}}{\tilde{k}} - \frac{\tilde{k}}{2}\right)\right], \quad g(x) = \int_0^\infty \frac{\xi d\xi}{\exp(\xi^2/2 - \epsilon_\mu) + 1} \ln\left|\frac{x+\xi}{x-\xi}\right|; \tag{28}$$

$$\varepsilon''_{\rm RPA}(\tilde{k},\tilde{\omega}) = \frac{\nu_0}{\tilde{k}^3} \ln\left\{\frac{1+\exp[\epsilon_\mu - 1/2(\tilde{\omega}/\tilde{k} - \tilde{k}/2)^2]}{1+\exp[\epsilon_\mu - 1/2(\tilde{\omega}/\tilde{k} + \tilde{k}/2)^2]}\right\}. \tag{29}$$

These formulas (28) and (29) are for plasmas at arbitrary degeneracy and were derived in [44]. For nondegenerate plasmas ($\epsilon_{\rm F} \ll 1$) they go into the form

$$\varepsilon'_{\rm RPA}(\tilde{k},\tilde{\omega}) = 1 + \sqrt{2}\frac{\tilde{\omega}_{\rm pl}^2}{\tilde{k}^3}\left[D\left\{\frac{1}{\sqrt{2}}\left(\frac{\tilde{\omega}}{\tilde{k}} + \frac{\tilde{k}}{2}\right)^2\right\} - D\left\{\frac{1}{\sqrt{2}}\left(\frac{\tilde{\omega}}{\tilde{k}} - \frac{\tilde{k}}{2}\right)^2\right\}\right], \tag{30}$$

$$\varepsilon''_{\rm RPA}(\tilde{k},\tilde{\omega}) = \sqrt{2}\frac{\tilde{\omega}_{\rm pl}^2}{\tilde{k}^3} \sinh\left(\frac{\tilde{\omega}}{2}\right) \exp\left[-\frac{1}{2}\frac{\tilde{\omega}^2}{\tilde{k}^2} - \frac{\tilde{k}^2}{8}\right], \tag{31}$$

where $D(x) = e^{-x^2}\int_0^x e^{t^2} dt$ is the Dawson integral.

The Drude-like expression (15) with the dynamical collision frequency (27) describes the permittivity in the whole frequency range. Particularly, it gives the plasmon peak near the plasma frequency $\omega_{\rm pl}$. Results very close to that obtained by Eq. (27), but with a lack of details for $\varepsilon(\omega)$ near $\omega = \omega_{\rm pl}$, can be obtained within a simpler approach by using a statically screened Coulomb potential (Debye potential) [43] in the Born approximation. Thus, one obtains

$$\tilde{\nu}_{\rm D}(\tilde{\omega}) = -\frac{i\nu_0 Z}{\tilde{\omega}} \int_0^\infty \frac{\tilde{k}^2[\varepsilon_{\rm RPA}(\tilde{k},\tilde{\omega}) - \varepsilon_{\rm RPA}(\tilde{k},0)]d\tilde{k}}{\left[1 + \tilde{k}_{\rm D}^2/\tilde{k}^2\right]^2}, \tag{32}$$

where $\tilde{k}_{\rm D}$ is the inverse screening length, as obtained for arbitrary degeneracy [20],

$$\tilde{k}_{\rm D}^2 = 3/4\left[\tilde{R}_{\rm D}^2 \epsilon_{\rm F}^{3/2}\right]^{-1} I_{-1/2}(\epsilon_\mu), \tag{33}$$

and $\tilde{R}_{\rm D} = R_{\rm D}/\lambda\!\!\!^{-}$ is the dimensionless Debye radius, with $R_{\rm D} = V_{\rm th}/\omega_{\rm pl}$.

Following [19], we write expression (32) in a more explicit form since similar expressions are obtained for higher order correlation functions,

$$\tilde{\nu}_{\rm D}(\omega) = i\omega_{\rm au} Z/(3\pi^2) \int_0^\infty dy f_{\rm scr}(y) \int_{-\infty}^\infty \frac{dx}{x} \times \frac{1}{w + i\delta - x} \ln\left[\frac{1 + e^{\epsilon_\mu - (x/y - y)^2}}{1 + e^{\epsilon_\mu - (x/y + y)^2}}\right], \tag{34}$$

where $w = \tilde{\omega}/4$, $y = \tilde{k}/(2\sqrt{2})$, and $f_{\rm scr}(y)$ is the screening function. The latter can be written for the case (32) of statical screening as

$$f_{\rm scr}(y) = y^3/\left[y^2 + \tilde{k}_D^2/8\right]^2. \tag{35}$$

Using the Sokhotski-Plemej formula $[w - x + i\delta]^{-1} = \frac{\mathcal{P}}{w-x} - i\pi\,{\rm Res}(x = w)$, the expressions for real and imaginary parts of $\tilde{\nu}_{\rm D}(\omega) = \tilde{\nu}'_{\rm D}(\omega) + i\tilde{\nu}''_{\rm D}(\omega)$ can be written as

$$\tilde{\nu}'_{\rm D}(\omega) = \frac{\omega_{\rm au} Z}{3\pi w} \int_0^\infty dy f_{\rm scr}(y) \ln\left[\frac{1 + e^{\epsilon_\mu - (w/y - y)^2}}{1 + e^{\epsilon_\mu - (w/y + y)^2}}\right], \tag{36}$$

$$\tilde{\nu}''_{\rm D}(\omega) = \frac{\omega_{\rm au} Z}{3\pi^2 w} \int_0^\infty dy f_{\rm scr}(y) \left[\sum_{\delta=\pm1} \mathcal{I}_{11}^\delta(y) - 2\mathcal{I}_{11}^0(y)\right], \tag{37}$$

$$\mathcal{I}_{11}^l = \int_0^\infty \frac{d\xi}{\xi} \sum_{\sigma=\pm1} \sigma \ln[1 + e^{\epsilon_\mu - [\xi + \sigma(y + lw/y)]^2}], \tag{38}$$

$l = 0, \pm 1$.

According to Eq. (19), the above expressions for $\nu_1(\omega)$ are equal to the correlation function $\mathfrak{C}_{11}(\omega)$ multiplied by $\omega_{\rm au}$. The expressions for correlation functions $\mathfrak{C}_{nm}(\omega)$ for n or (and) $m > 1$ in a screened Born (or Debye) approximation have a form similar to Eq. (34) (see Ref. [19]) and are given in Appendix B.

D. Effective screening parameter

In this section we show how the inverse screening length for statical screening (35) can be derived from expression (27) for the case of dynamical screening. In addition, this approach gives us the possibility to introduce dynamical screening into higher order correlation functions (B1) and (B6). Using a formal comparison of (27) with (32), keeping in mind the definition of the screening function (35), we get an expression for the screening function in the case of dynamical screening,

$$f_{\rm scr}(y,w) = \varepsilon^{*}_{\rm RPA}(y,w)/[y\varepsilon'_{\rm RPA}(y,0)|\varepsilon_{\rm RPA}(y,w)|^2], \quad (39)$$

where $\varepsilon_{\rm RPA}$ is the RPA permittivity (28) and (29), which in new variables can be rewritten in an equivalent form as

$$\varepsilon_{\rm RPA}(y,w) = 1 + \frac{\sqrt{\tilde{\omega}_{\rm au}}}{8\sqrt{2}\pi}\frac{1}{y^3}\left[-\sum_{\delta=\pm1}\mathcal{I}^{\delta}_{11}(y) + i\pi\ln\left\{\frac{1+\exp[\epsilon_\mu-(w/y-y)^2]}{1+\exp[\epsilon_\mu-(w/y+y)^2]}\right\}\right], \quad (40)$$

where $\mathcal{I}^{\pm1}_{11}$ is given by (38).

Keeping in mind that in the considered case of dynamical screening the screening function $f_{\rm scr}(y,w)$ (39) is a complex function [45], one can rewrite the expressions for real and imaginary parts of the correlation functions stipulated by electron-ion interactions as

$$\begin{aligned}\mathfrak{C}'\mathrm{ei}_{nm} &= \mathfrak{C}'\mathrm{ei}_{nm}(f'_{\rm scr}) - \mathfrak{C}''\mathrm{ei}_{nm}(f''_{\rm scr}),\\ \mathfrak{C}''\mathrm{ei}_{nm} &= \mathfrak{C}''xg\mathrm{ei}_{nm,\mathrm{D}}(f'_{\rm scr}) + \mathfrak{C}'\mathrm{ei}_{nm}(f''_{\rm scr}),\end{aligned} \quad (41)$$

where designations $\mathfrak{C}'^{\rm ei}_{nm}(f'_{\rm scr})$ and $\mathfrak{C}''^{\rm ei}_{nm}(f'_{\rm scr})$ (where superscripts "ei" designate e-i interactions) mean that in the respective expressions (B5) and (B6) for real and imaginary parts of correlation functions the real part of screening function (39) is substituted for $f_{\rm scr}$ and, similarly, designations $\mathfrak{C}'^{\rm ei}_{nm}(f''_{\rm scr})$ and $\mathfrak{C}''^{\rm ei}_{nm}(f''_{\rm scr})$ mean substitution of the imaginary part of $f_{\rm scr}$ (39).

One can show from Eqs. (39) and (40) that in the nondegenerate low-frequency case, i.e., at $\epsilon_{\rm F} \ll 1$ and $w \ll 1$,

$$f_{\rm scr} \approx \frac{y^3}{\left[y^2 + 1/\left(8\tilde{R}^2_{\rm D}\right)\right]^2}\left[1 - i\frac{\sqrt{\pi}\,w/y}{1+8\tilde{R}^2_{\rm D}y^2}\right], \quad (42)$$

and in the degenerate low-frequency case, i.e., at $\epsilon_{\rm F} \gg 1$ and $w \ll 1$,

$$f_{\rm scr} \approx \frac{y^3}{\left[y^2 + 3/\left(16\tilde{R}^2_{\rm D}\epsilon_{\rm F}\right)\right]^2}\left[1 - i\frac{3\pi\,w/(2y\sqrt{\epsilon_{\rm F}})}{3+16\tilde{R}^2_{\rm D}y^2\epsilon_{\rm F}}\right]. \quad (43)$$

In the low-frequency case the main contribution to the integrals like (B5) and (B6) comes from $y \sim \sqrt{w} \ll 1$; hence, one can disregard the imaginary parts in Eqs. (42) and (43) and use the following expression in (35) to ensure proper interpolation between (42) and (43),

$$\tilde{k}^2_{\rm D} \approx \tilde{k}^2_{\rm D,deg} = \left[\tilde{R}^2_D(1+2\epsilon_{\rm F}/3)\right]^{-1}, \quad (44)$$

which also gives an interpolation of Eq. (33). It ensures good agreement between calculations using expressions (27) and (32); see Sec. IV below. A similar expression $\tilde{k}^2_{\rm D} = \tilde{R}_{\rm D}^{-2}/[1+\epsilon_{\rm F}^4]^{1/4}$ was introduced in Ref. [46], but it gives wrong asymptotics at low temperatures and less agreement when comparing with results obtained from Eqs. (27) and (32).

For strongly coupled plasmas, the perturbative approach, which is the basis for LRT, is, generally speaking, not valid. In this case, the screening parameter can be different from that described above. In Ref. [35] it was argued that one should use the maximum of the Debye length and interatomic distance (3) as screening length in dense coupled plasmas. That means that formula (44) in strongly coupled plasmas could be rewritten as

$$\tilde{k}^2_{\rm D} = \min\left\{\tilde{k}^2_{\rm D,deg}, \tilde{k}^2_{\rm max}\right\}, \quad (45)$$

$$\tilde{k}^2_{\rm max} = 8\epsilon_{\rm F}/(18\pi Z)^{2/3}. \quad (46)$$

Keeping in mind (45) and (35), one can suppose that in the case of dynamical screening (39) the screening function $f_{\rm scr}$ will also be restricted from below by the value

$$f_{\rm scr,min} = y^3/\left[y^2 + \tilde{k}^2_{\rm max}/8\right], \quad (47)$$

where $\tilde{k}_{\rm max}$ is given by Eq. (46).

The importance of taking into account the screening of the Coulomb potential was underlined in a recent paper [47]. Unlike Ref. [47], our approach permits to take into account different versions of screening and does not need special "Drude-like infrared regularization" [48,49] at small frequencies of radiation.

It is interesting to note that expression (44) can be rewritten as

$$\tilde{k}^2_{\rm D,deg} = \frac{8\Gamma_{ei}}{(2\sqrt{3\pi}\,Z)^{2/3}}\frac{\epsilon_{\rm F}}{1+2\epsilon_{\rm F}/3}. \quad (48)$$

In Sec. III A below, we derive an expression for the generalized electron-ion coupling parameter $\Gamma_{\rm deg}$. Keeping in mind the relation (76) given there, one can conclude from expressions (46) and (48) that the restrictions of screening occur at

$$\Gamma_{\rm deg} > 1/3.$$

E. High-frequency asymptotics and inverse bremsstrahlung

For $\tilde{\omega} \gg \epsilon_\mu$ and $\tilde{\omega} \gg \tilde{\omega}_{\rm pl}$ it can be shown that one can disregard $\tilde{k}^2_{\rm D}$ in Eq. (36) (the respective terms are exponentially small, $\sim e^{\epsilon_\mu - w}$) and rewrite it as

$$\tilde{\nu}'_{\rm D}(\omega) = \frac{\omega_{\rm au}Z}{3\pi\,w}\int_0^\infty\frac{dy}{y}\ln\left[\frac{1+e^{\epsilon_\mu-(w/y-y)^2}}{1+e^{\epsilon_\mu-(w/y+y)^2}}\right]. \quad (49)$$

With account of the inequality $w \gg 1$, the expression (49) can be simplified and written in terms of an asymptotic series with respect to the parameter w^{-1}. With account for only leading order terms this can be written as [50]

$$\tilde{\nu}'_{\rm D}(\omega) = \frac{\tilde{\omega}_{\rm au}Z}{3\pi\,w^{3/2}}\int_{-\infty}^{\infty}dt\,\ln[1+e^{\epsilon_\mu-4t^2}] \quad (50)$$

for the case of arbitrary degeneracy or

$$\tilde{\nu}'_{\rm D}(\omega) \approx \frac{2\tilde{\omega}_{\rm au} Z \epsilon_\mu^{3/2}}{9\pi w^{3/2}} \left[1 + \frac{\pi^2}{8\epsilon_\mu^2} + \frac{7\pi^4}{640\epsilon_\mu^4} \right] \tag{51}$$

for the highly degenerate case $\epsilon_\mu > 1$.

From (49) one immediately can obtain the well-known expression [53] for nondegenerate plasmas

$$\tilde{\nu}'_{\rm D}(\omega) = \frac{32\tilde{\omega}_{\rm au} Z}{9\pi^{3/2}\tilde{\omega}} \epsilon_{\rm F}^{3/2} \sinh\left(\frac{\tilde{\omega}}{2}\right) K_0\left(\frac{\tilde{\omega}}{2}\right), \tag{52}$$

where $K_0(x) = \int_0^\infty dt \exp[-x\cosh(t)] = \int_0^\infty dy \exp[-y^2 - x^2/(4y^2)]/y$ is the modified Bessel function of the second kind. Keeping in mind the limit $\tilde{\omega} \gg 1$, one can derive from (52) the following asymptotic:

$$\tilde{\nu}'_{\rm D}(\omega \gg 1) = \frac{16\tilde{\omega}_{\rm au} Z}{9\pi\tilde{\omega}^{3/2}} \epsilon_{\rm F}^{3/2}. \tag{53}$$

This expression coincides with the first term of a similar expression for degenerate plasmas, Eq. (51), if one takes into account that $w = \tilde{\omega}/4$ and $\epsilon_\mu \approx \epsilon_{\rm F}$ for the degenerate case.

For the imaginary part of the permittivity and large $\tilde{\omega}$ one has from Eq. (37) the expression

$$\tilde{\nu}''_{\rm D}(\omega) = -\frac{8\tilde{\omega}_{\rm au} Z}{3\pi^2\tilde{\omega}} \int_0^\infty dy\, f_{\rm scr}(y)\, \mathcal{I}_{11}^0(\epsilon_\mu, y), \tag{54}$$

where $\mathcal{I}_{11}^0$ is given by Eq. (38); it does not depend on ω.

The dielectric function $\varepsilon(\omega) = [n(\omega) + ic/(2\omega)\alpha(\omega)]^2$ determines the refraction index $n(\omega)$ as well as the absorption coefficient $\alpha(\omega)$, which is related in thermal equilibrium with emission coefficient $j(\omega)$ by Kirchhoff's law of radiation $j(\omega) = \alpha(\omega) L_\omega(\omega)$, where $L_\omega(\omega)$ is the spectral power density of blackbody radiation.

In the high-frequency limit, where $n(\omega) \approx 1$ and $\omega \gg \nu'_{\rm D}$, one has

$$\alpha(\omega) = \frac{\omega}{c\, n(\omega)} {\rm Im}\, \varepsilon(\omega) \approx \frac{\omega_{\rm pl}^2}{\omega^2 c} \nu'_{\rm D}(\omega), \tag{55}$$

so that the inverse bremsstrahlung absorption coefficient is directly related to the real part of the dynamical collision frequency obtained above.

Using Eqs. (55) and (52) in the nondegenerate limit, one can write an expression for $\alpha(\omega)$ in the form

$$\frac{c\hbar\alpha}{T} = \frac{32}{9}\sqrt{\frac{\pi}{3}} Z \frac{\omega_{\rm au}\omega_{\rm pl}^2}{\omega^3} \epsilon_{\rm F}^{3/2} (1 - e^{-\tilde{\omega}}) g_{ff}^{\rm Born}(\omega),$$
$$g_{ff}^{\rm Born} = (\sqrt{3}/\pi^2) \exp(\tilde{\omega}/2) K_0(\tilde{\omega}/2), \tag{56}$$

where $g_{ff}^{\rm Born}$ is the free-free Gaunt factor in Born approximation; see Refs. [20,54–56].

The expression (56) coincides with the result derived in [53] and with the well-known Bethe-Heitler expression resulting from QED in second order of interaction [57] for a hydrogen plasma in the nonrelativistic limit.

The well-known Kramers formula for the inverse bremsstrahlung absorption [58] results with the Gaunt factor $g_{ff}^{\rm Kramers}(\omega) = 1$. The same approximation for the Gaunt factor was used in a recent paper [47].

This one-moment Born approximation can be improved taking into account dynamical screening, strong collisions, and higher moments in the statistical operator, as discussed earlier. However, in the high-frequency limit, the dynamical screening is not of relevance. Similarly, the renormalization factor $r_\omega(\omega) \to 1$ for $\omega \gg \omega_{\rm pl}$; see Refs. [19,20] and Fig. 3 below.

Strong collisions have been considered and lead to the famous Sommerfeld result for the Gaunt factor [54,59]. For dense plasmas, the account of ion correlation has a major effect and can be directly included in the Born approximation [60] via the static structure factor $S_{\rm ii}(\tilde{k})$; see Sec. II G below.

The standard treatment of the kinetic equation using a relaxation time ansatz (see Sec. III) fails to describe inverse bremsstrahlung absorption at high frequencies. The frequently used classical kinetic expression for the dynamical conductivity, or the corresponding expression for the dielectric function, is restricted to the low-frequency region since a static, p-dependent (and ω-independent) relaxation time cannot be applied to the high-frequency region. Different approaches using Fermi's golden rule have been used [53,61] to derive expressions for the emission of radiation. A common treatment unifying both limiting cases, $\omega \to 0$ and $\omega \to \infty$, is missing in KT if the relaxation time approximation is used.

In contrast, our approach within LRT covers the entire frequency regime consistently, is applicable to the degenerate case [62], and can also be applied to the relativistic regime [63]. An important feature of the LRT is the possibility to include medium effects in dense plasmas such as the Landau-Pomeranchuk-Migdal effect [55,56].

F. Low-frequency asymptote

For $\tilde{\omega} \ll 1$ one has the asymptotic behavior from expressions (B5) and (B6),

$$\mathfrak{C}'^{eq}_{nm}(\tilde{\omega}) = \frac{4\alpha_q}{3\pi} \int_0^\infty f^q_{\rm scr}(y) R^{eq}_{nm}(0,y) \frac{e^{\epsilon_\mu - y^2} dy}{1 + e^{\epsilon_\mu - y^2}}, \tag{57}$$

$$\mathfrak{C}''^{eq}_{nm}(\tilde{\omega}) = \frac{w\alpha_q}{3\pi^2} \int_0^\infty \frac{dy}{y^2} f^q_{\rm scr}(y) \int_0^\infty \frac{d\xi}{\xi} \sum_{\sigma=\pm1} \sigma \times \frac{\partial^2}{\partial\xi^2} \left\{ R^{eq}_{nm}(\xi, y) \ln[1 + e^{\epsilon_\mu - (\xi + \sigma y)^2}] \right\}, \tag{58}$$

where superscripts "eq" designate e-e or e-i interactions; $w = \tilde{\omega}/4$.

From these expressions it is seen, that the real part of the correlation functions is independent of ω, while the imaginary part is vanishing proportional to ω.

Disregarding the small imaginary part $\mathfrak{C}''^{ei}_{11}$, one obtains from (57) and (18) an expression for the dynamical collision frequency ν by LRT in the considered low-frequency limit,

$$\nu(\tilde{\omega} \ll 1) \approx \nu_{\rm pl,0}\, r'_\omega\, \Lambda_{\rm LRT}, \quad \nu_{\rm pl,0} = \frac{4\sqrt{2\pi}}{3} \frac{n_e e^4 Z}{\sqrt{m} T^{3/2}}, \tag{59}$$

where r'_ω is the real part of renormalization factor and

$$\Lambda_{\rm LRT} = \frac{3\sqrt{\pi}/4}{\epsilon_{\rm F}^{3/2}} \int_0^\infty f_{\rm scr}(y) \frac{e^{\epsilon_\mu - y^2}}{1 + e^{\epsilon_\mu - y^2}} dy \tag{60}$$

is the Coulomb logarithm. In the nondegenerate case and with expression (44) for $f_{\rm scr}$ one has from (60) the expression

$$\Lambda_{\rm LRT}(\epsilon_{\rm F} \ll 1) \approx (\ln \varkappa^{-1} - C - 1)/2, \quad \varkappa = \tilde{k}_{\rm D}^2/8, \qquad (61)$$

coincident with the Brooks-Herring Coulomb logarithm [64], where $\tilde{k}_{\rm D}^2/8$ is given by (44) and (48) and $C \approx 0.5772$ is Euler's constant.

G. Ion correlations and screening

We now consider the incorporation of ion correlations explicitly according to Eq. (2) via the static structure factor. For the estimation of the ion structure factor for noncrystalline materials, like liquid metals or dense plasmas, an analytical model [65,66], derived within a one-component plasma model, can be used,

$$S_{\rm ii}(k) = \Big\{1 - \frac{3\Gamma_{\rm ii}}{(kR_0)^4 a_2^2}[\cos(kR_0a_1) + 2\cos(kR_0a_2) - 3\sin(kR_0a_1)/(kR_0a_1)]\Big\}^{-1}, \qquad (62)$$

$$a_1 = -0.1455 \times 10^{-2}\Gamma_{\rm ii} + a_{1Z}(Z),$$

$$a_{1Z}(Z) = \begin{cases} 0.96, & Z = 1, \\ 1.0, & Z = 2, \\ 1.08, & Z = 3, \\ 1.15, & Z \geqslant 4, \end{cases} \quad a_2(Z) = \begin{cases} 1.45, & Z = 1, \\ 1.80, & Z = 2, \\ 2.10, & Z = 3, \\ 2.25, & Z \geqslant 4, \end{cases}$$

where $\Gamma_{\rm ii} = (Ze)^2/(R_0T_{\rm i})$ and R_0 is interatomic distance, see Eq. (3) above. Since this model does not incorporate properties of specific metals, it can be used for an estimation of the ion structure factor $S_{\rm ii}$ for WDM, including Al plasmas.

Besides ion correlations, it is important to take into account the influence on the permittivity of warm dense matter caused by the screening of the Coulomb potential and Pauli blocking due to the interaction with bound and valence electrons near the nucleus [46] of complex ions. This can be done by introducing some pseudopotential instead of the Coulomb potential of the ion. The most simple form of such a pseudopotential is the empty core potential [46,67] in the form

$$V_{\rm ei}(r) = \begin{cases} Ze^2/r & \text{for} \quad r > r_{\rm cut}\,, \\ 0 & \text{for} \quad r \leqslant r_{\rm cut}\,, \end{cases} \qquad (63)$$

where the radius $r_{\rm cut}$ is treated as a free parameter which can be fitted to match experimental data on transport and optical properties. Keeping in mind the respective expression for the Fourier transform of the potential (63) (see Ref. [46]), one gets a modified expression for the screening function $f_{\rm scr}(y)$ [remember that $y = \tilde{k}/(2\sqrt{2})$], which takes into account the difference between the screening function for the pure Coulomb potential and the potential (63) in the expressions for correlation functions containing the interactions between electrons and ions,

$$f_{\rm scr}^{\rm ei}(y) = f_{\rm scr}(y)\cos^2(2\sqrt{2}y\tilde{r}_{\rm cut}). \qquad (64)$$

In the case of complex ions expression (64) is taken for $f_{\rm scr}^{\rm i}$ in expressions (B5) and (B6) for the e-i-correlation functions.

III. DIELECTRIC FUNCTION FROM KINETIC THEORY

A. Effective collision frequency

The more simple, though less common, treatment of plasma permittivity can be done using kinetic equations for the single-particle electron distribution function. In Ref. [19] it was demonstrated that quantum kinetic equations can be derived within the scope of quantum statistical theory and hence it is formally equivalent to the method of quantum statistical operator used above.

On the other hand, frequently used classical kinetic equations within relaxation time approximation [23] are, generally speaking, applicable only for low-frequency perturbations, as long as the electron-ion collisions in relaxation time approximation are independent on frequency. Nevertheless, due to its simplicity this method is widely used in hydrodynamic codes and also it is convenient for the construction of semiempirical models based on experimental data [9,10,13].

A slightly more complex, but still elementary, approach is based on an approximate solution of the Fokker-Planck equation as proposed in Ref. [68]. This permits to take into account not only the contribution of electron-ion collisions to the DF $\varepsilon(\omega)$ (as in the case of relaxation time approximation), but also the electron-electron collisions. In accordance with [68], the permittivity of plasmas due to intraband transitions is expressed as

$$\varepsilon(\omega) = 1 - (\omega_{\rm pl}/\omega_0)^2\mathcal{K}_0(\omega), \qquad (65)$$

$$\mathcal{K}_0 = \frac{-2i\chi_Z}{\xi_\omega \varepsilon_{\rm F}^{3/2}} \int_0^\infty F(1;\alpha_Z; i\beta_Z\xi^3) f_{\mathcal{F}}(\xi)[1 - f_{\mathcal{F}}(\xi)]\xi^7 d\xi, \qquad (66)$$

where the function $\mathcal{K}_0$ is expressed in terms of the confluent hypergeometric function $F(a;b;z)$; $\chi_Z = [1 + 5/Z_*]^{-1}$, $\xi_\omega = (3\sqrt{\pi}/4)(\nu_{\rm eff}^{\rm nd}/\omega)$, $\xi = v/(\sqrt{2}V_{\rm th})$, $\alpha_Z = (Z_* + 8)/3, \beta_Z = Z_*/(3\xi_\omega)$; the Fermi function $f_{\mathcal{F}}(\xi) = [1 + \exp(\xi^2 - \epsilon_\mu)]^{-1}$; and $Z_* = Z/\varkappa$ is an effective charge. The function $\varkappa$ is constructed in such a way [68] that limits at high and low laser frequencies and for nondegenerate [69], as well as for degenerate [34], matter are fulfilled,

$$\varkappa(\omega) = \varkappa_0/[1 + (C/\xi_\omega)^s], \quad \varkappa_0 = Z\big[\widetilde{\gamma}_\sigma^{-1}(Z) - 1\big]/5,$$
$$\widetilde{\gamma}_\sigma = \gamma_\sigma(Z) + \frac{1 - \gamma_\sigma(Z)}{1 + 0.6\ln[1 + (20\epsilon_{\rm F})^{-1}]}, \quad \gamma_\sigma = \frac{a + Z}{b + Z}, \qquad (67)$$

where the constants were determined as $a = 0.87$, $b = 2.2$, $C = s = 1$. The value

$$\nu_{\rm eff}^{\rm ndeg} = \nu_{\rm pl,0}\,\Lambda \qquad (68)$$

is an *effective electron-ion collision frequency for nondegenerate plasma*, expressed in terms of the Coulomb logarithm Λ, which can be determined in a wide range of plasma parameters by respective interpolation formulas [34,35,68,70]; see Sec. III B.

The above formulas ensure proper well-known high- and low-frequency skin effect asymptotes for nondegenerate [25,69] and for degenerate Lorentz plasmas [71–74]

(disregarding electron-electron collisions). Therefore, the calculation of optical properties is possible for matter in a wide range of parameters of laser and plasmas with arbitrary ion charge.

We now analyze further the general expression (66). A power series expansion of F with respect to its third argument for the case $\beta_Z \xi^3 \ll 1$ reads

$$F(1;\alpha_Z;i\beta_Z\xi^3) = 1 + i\frac{\beta_Z\xi^3}{\alpha_Z} - \frac{\beta_Z^2\xi^6}{\alpha_Z(\alpha_Z+1)} + \cdots, \quad (69)$$

and the asymptotic expansion of F in the limit $Z_* \gg 1$ reads

$$F(1;\alpha_Z;i\beta_Z\xi^3) = \frac{1}{1-\widetilde{\beta}_Z} + \sum_{n\geqslant 1}\frac{1}{Z_*^n}\frac{\widetilde{\beta}_Z P_n(\widetilde{\beta}_Z)}{(1-\widetilde{\beta}_Z)^{2n+1}}, \quad (70)$$

where $\widetilde{\beta}_Z = i\xi^3/\xi_\omega$ and $P_n(\widetilde{\beta}_Z)$ are polynomials of $\widetilde{\beta}_Z$ to the nth power [68].

Taking only the first term in the expansion (70), in the leading order one gets from (66) the expression

$$\mathcal{K}_0(\omega) = \frac{2}{\varepsilon_F^{3/2}}\int_0^\infty \frac{f_{\mathcal{F}}(\xi)[1-f_{\mathcal{F}}(\xi)]}{\xi^3 + i\xi_\omega}\xi^7 d\xi, \quad (71)$$

which coincides with a result obtained earlier [25,71–73,75] for the electron conductivity of the Lorentz plasma.

From Eqs. (70) and (66) one gets the expression

$$\mathcal{K}_0(\omega) = 1 - i\,\chi_{Z_3}\xi_\omega\varepsilon_F^{-3/2}(1+e^{-\epsilon_\mu})^{-1} \quad (72)$$

in the high-frequency limit $\omega \gg \nu_{\rm eff}$. From Eqs. (69) and (66) one gets the expression

$$\mathcal{K}_0(\omega) = \frac{3\chi_{Z_1}}{\xi_\omega^2}\frac{I_{7/2}(\epsilon_\mu)}{I_{1/2}(\epsilon_\mu)} - \frac{2i\,\chi_Z}{\xi_\omega}\frac{I_2(\epsilon_\mu)}{I_{1/2}(\epsilon_\mu)} \quad (73)$$

for low frequencies $\omega \ll \nu_{\rm eff}$, where $\chi_{Z_3} = 1 + 2/Z_*$ and $\chi_{Z_1} = (1+5/Z_*)^{-1}(1+8/Z_*)^{-1}$.

From Eq. (72) it follows [76] that in a wide range of degeneracy parameter the effective electron collision frequency, which determines the dynamical conductivity and the absorption in kinetic models, can be expressed in the form

$$\nu_{\rm eff} = \frac{3\sqrt{\pi}\,\nu_{\rm pl,0}}{4\epsilon_F^{3/2}}\frac{1}{1+e^{-\epsilon_\mu}}\Lambda, \quad (74)$$

which reproduces known limiting cases for nondegenerate and highly degenerate plasmas [68,76], in particular, Eq. (68) for a nondegenerate plasmas.

One can rewrite (74) in the form

$$\nu_{\rm eff} = \sqrt{2/(3\pi)}\,\omega_{\rm pl}\Gamma_{\rm deg}^{3/2}\Lambda(\Gamma_{\rm deg}, Z, \varrho), \quad (75)$$

where

$$\Gamma_{\rm deg} = \frac{\Gamma_{\rm ei}}{\epsilon_F[4(1+e^{-\epsilon_\mu(\epsilon_F)})/(3\sqrt{\pi})]^{2/3}} \quad (76)$$

is the generalized electron-ion coupling parameter for plasma at arbitrary degeneracy. In the nondegenerate case, (76) is the usual expression $\Gamma_{\rm deg} \approx \Gamma_{\rm ei} = Ze^2/(R_0T)$. In the case of strongly degenerate ($\epsilon_F \gg 1$) plasmas, the respective coupling parameter depends on the Fermi energy, $\Gamma_{\rm deg} \approx (9\pi/16)^{1/3}Ze^2/(R_0E_F) = 1.21Ze^2/(R_0E_F)$.

Alternatively, expression (76) can be rewritten as

$$\Gamma_{\rm deg} = 2^{-1/6}Z^{2/3}(\hbar\omega_{\rm au}/T)^{1/2}D_\Gamma(\Theta), \quad (77)$$

$$D_\Gamma = \Theta^{1/2}\{1+\exp[-X_{1/2}(2\Theta^{-3/2}/3)]\}^{-1}. \quad (78)$$

The function $D_\Gamma(\Theta)$ has a minimum at $\Theta = \Theta_* \approx 0.519$, with $D_\Gamma(\Theta_*) \approx 1.514$. It is slowly varying in the vicinity of Θ_* [$D_\Gamma \in (1.51; 1.72)$ for $\Theta \in (0.27; 0.94)$]. From this fact and Eq. (75) it follows that in strongly coupled plasmas the effective collision frequency is proportional to the plasma frequency,

$$\nu_{\rm eff,max} = {\rm k}_1\omega_{\rm pl}, \quad (79)$$

with some numerical coefficient $\rm k_1$, which is in the order of 1. Effectively, the maximum of the effective collision frequency is a function of the plasma density. The actual value of $\rm k_1$ can be determined from the comparison with experimental data [9,10,76].

It should be noted that if one takes into account not only electron-ion and electron-electron scattering, as in the above consideration, but also electron-phonon interaction and umklapp processes [77], then the effective frequency of collisions and absorption will have some maximum as a function of the electron temperature [9,13,78].

B. Coulomb logarithm

From the considerations given above it is clear that the differences of various kinetic and semiempirical models in determining the laser energy absorption are crucially dependent on the determination of the the Coulomb logarithm Λ, which is a slowly varying function of density and temperature. Different authors give different expressions for Λ within the quantum or the classical kinetic approach. Below, some of them are briefly considered.

A well-known wide-range model for Λ was proposed in [71]. This model was refined by different authors who had proposed expressions that show better agreement with experimental data. A common expression for Λ can be written as

$$\Lambda = C_{\Lambda,0}\ln[1 + (C_{\Lambda,1}b_{\rm max}/b_{\rm min})^{1/C_{\Lambda,0}}], \quad (80)$$

where $C_{\Lambda,0}$ and $C_{\Lambda,1}$ are constants and $b_{\rm max}$ and $b_{\rm min}$ are maximum and minimum impact parameters.

An approximation for Λ, which is accurate up to nonlogarithmic terms, was suggested in [35] for weakly coupled, high-temperature, low-density, high-Z plasmas (with $b_{\rm max}/b_{\rm min} \gg 1$). Extending the interpolation formula proposed in [35] to the case of moderately coupled plasmas, one can rewrite it in the form (80), with

$$b_{\rm max} = \min\{\max\{\lambda_D, R_0\}, V_{\rm th}/\omega\},$$
$$b_{\rm min} = \max\{b_{90}(v_1), \lambda_q(v_1)\}, \quad (81)$$

where $v_1 = \sqrt{3}V_{\rm th}$, $b_{90}(v) = Ze^2/(mv^2)$ is the impact parameter for 90° scattering, and $\lambda_q(v) = \hbar/(2mv)$ is the quantum-mechanical minimum impact parameter. The screening length

$$\lambda_D = R_D/\sqrt{1/(1+2\epsilon_F/3) + ZT/T_i}, \quad (82)$$

accounts for both the electrons' degeneracy [79] via the term $(1+2\epsilon_F/3)^{-1}$ [see (45)] and screening by ions via the term ZT/T_i.

The constant $C_{\Lambda,0}$ in Eq. (80) is usually taken as $C_{\Lambda,0}=1/2$, which leads to the result obtained from the classical trajectory approximation [35,71,80]. Another choice $C_{\Lambda,0}=2/3$ ensures proper high-frequency asymptotics (see Sec. II E) of the real part of the permittivity. The term V_{th}/ω in (81) represents the Dawson-Oberman (DO) correction to the dynamical conductivity in the high-frequency case [81,82]. The numerical coefficient of this term was substantiated in [35].

The constant $C_{\Lambda,1}$ in Eq. (80) is determined by the high-temperature asymptotics, where $b_{max}/b_{min}\gg 1$ and $\Lambda\approx \ln(b_{max}/b_{min})+\ln(C_{\Lambda,1})$. In [35] the value of $C_{\Lambda,1}\approx 0.287$ was proposed. However, in [35] only weakly coupled, high-temperature plasmas were considered. The consideration of moderately coupled plasmas shows that $C_{\Lambda,1}\approx 1$ will be a better choice. More precisely, calculations presented below have shown that a better agreement between results of the kinetic approach considered here with the QS ones are obtained with $C_{\Lambda,1}=1$ for frequencies $\omega<\omega_{pl}$ and $C_{\Lambda,1}=0.5$ for frequencies $\omega\gg\omega_{pl}$. We propose the expression

$$C_{\Lambda,1}\approx 1-0.25[\tanh(\omega/\omega_{pl}-5)+1], \tag{83}$$

which interpolates between limits $C_{\Lambda,1}=1$ and $C_{\Lambda,1}=0.5$ and is applicable in the entire frequency range.

The expressions (80) and (81) have been obtained following the relaxation time approximations of the respective integrals over the velocity space with the electron distribution function. More general expressions can be obtained for a velocity-dependent Coulomb logarithm, which can be expressed as [83]

$$\Lambda(v)=\frac{1}{2}\left[\ln(1+Q)-\frac{Q}{1+Q}-\frac{1}{2}\frac{Q^2}{(1+Q)^2}\right], \tag{84}$$

where $Q=[\lambda_D/b_{min}(v)]^2$ and $b_{min}(v)$ is given by (81), but with the replacement $v_1\leftrightarrow v$.

The DO-like correction can also be introduced in (84) by replacing the above expression for Q by

$$Q=\min\{[\lambda_D/b_{min}(v)]^2,8/\tilde{\omega}^2\}. \tag{85}$$

The expression (84) with only the first and second terms on the right side was derived, for example, in [19] within the first Born approximation using the quantum kinetic equation and the screened Coulomb potential ($b_{min}=\lambda_q(v)$, i.e., the quantum-mechanical limit was used in Ref. [19]). The third term in (84) arises if one takes into account ionic correlations [80,84] (in [80] the classical limit $b_{min}=b_{90}$ was used).

The expression (84) cannot be extrapolated into the high-frequency region by a simple replacement of λ_D with v/ω, like in Eq. (81). In particular, for small Q (corresponding to large ω) one has from (84) $\Lambda(v)\sim Q^2\sim\omega^{-4}$ in the case when we consider only the first two terms on the right-hand side or $\Lambda(v)\sim Q^3\sim\omega^{-6}$ in the case of three terms. Note that the correct asymptote $\Lambda(v)\sim\omega^{-3/2}$ for $\omega\gg\omega_{pl}$ follows from comparison of Eqs. (68) and (50).

In Ref. [34] an expression for the Coulomb logarithm is derived in second Born approximation. It can be written in the form

$$\Lambda=\ln\left(\frac{b_{mx1}}{\lambda_{q*}}\right)-\frac{1}{2}+\frac{2b_{90*}}{b_{mx1}}\left[\ln\left(\frac{b_{mx1}}{\lambda_{q*}}\right)-\ln 2^{4/3}\right], \tag{86}$$

where $b_{mx1}=\max\{\lambda_D,R_0\}$, $\lambda_{q*}=\hbar/(2mv_*)$, $b_{90*}=Ze^2/(mv_*^2)$, and $v_*=\sqrt{(7T+2E_F)/m}$ [85]. In accordance with [34], expression (86) is valid for moderately coupled plasmas, when $\Gamma_{ei}<1$. The extrapolation of expression (86) to the high-frequency case is also difficult because of nonlogarithmic terms, which leads to negative values for Λ.

Calculations according to the models discussed above are considered in the following section. Before, however, it is instructive to compare LRT and KT results for the case of small frequencies $\tilde{\omega}\ll 1$, when the dynamical collision frequency ν, calculated by LRT, can be approximated by expression (59). With the additional requirement $|\nu|\ll\omega$, the function $\mathcal{K}_0$ [see Eq. (65)] calculated by LRT can be written as $\mathcal{K}_0\approx 1-i\nu'/\omega$ with ν' given by Eq. (59). In the same domain of parameters, the function $\mathcal{K}_0$ calculated by KT is given, in accordance with (72) and (74), as $\mathcal{K}_0\approx 1-i\nu_{eff}/\omega$. The permittivities calculated by LRT and KT have the same functional form. They differ in the expression for the Coulomb logarithm. The similarity is especially obvious in the nondegenerate case.

Furthermore, the formal condition for the applicability of the Born approximation used in the above formulas (15), (18), (19), and (B5)–(B7) for LRT is $mv^2/2>Ze^2/[\hbar/(mv)]$, where $v\approx\sqrt{3T/m}$ is the average electron velocity, or $T>(4/3)Z^2E_H$, or $2.5\,\Gamma_{ei}^2\Theta Z^{2/3}<1$. This case corresponds to the condition $b_{min}=\lambda_q(v)$ in expression (81) for the minimum impact parameter ("quantum mechanical limit" [35]). As shown in [35], the KT model leading to Eqs. (80)–(82) can cover the full domain of the parameter $\Gamma_{ei}^2\Theta Z^{2/3}$, i.e., is formally applicable in both classical [$b_{min}=b_{90}(v)$] and quantum [$b_{min}=\lambda_q(v)$] limits. On the other hand, as it was shown above, LRT is applicable in a wide frequency range, while KT is well grounded only for low frequencies $\omega\ll\omega_{pl}$; see Sec. IV C below.

It is important to note that even at $T<(4/3)Z^2E_H$ the results for the permittivity from LRT are very close to the ones obtained by KT with semiempirical expressions for the effective collision frequency if $\omega\ll\omega_{pl}$, i.e., in the frequency range of the applicability of KT; see Sec. IV below. That means that the LRT constructed above can be used for the extension of the KT to be used in a wider frequency range.

IV. RESULTS OF CALCULATIONS

In this section we present an extensive comparison of numerical results calculated for the LRT and KT approaches. For the consistency of the LRT calculations, the Kramers-Kronig relations and sum rules [41] were checked numerically for such conditions as considered in the following sections. We looked at solid-density aluminum plasmas ($\rho=2.7$ g cm^{-3}) for different temperatures ($T=2,20,300$ eV). The accuracy of the s-sum rule was better than 0.4% for $T=2,20$ eV and 0.6% for $T=300$ eV. The accuracy of the f-sum rule was better than 0.4% for $T=2$, 20 eV and 1% at $T=300$ eV. The Kramers-Kronig relations were checked using the frequency range $\hbar\omega\in[0.01;2000]$ eV. The error was found

TABLE I. Different models as used in the calculations with a brief description are given. Restrictions for the applicability are indicated.

Abbreviation	Description of the model	Restrictions of the model
SB-1(2)	LRT model (15), (18), (19), (B3)–(B7), 1(2)-moment approach (using $\boldsymbol{P}_1$ or $\boldsymbol{P}_1$ and $\boldsymbol{P}_3$), within statically screened Born approximation (44)	$\Gamma_{ei} < 1$, formal condition of applicability is $T > (4/3)Z^2 E_H$ or $2.5\,\Gamma_{ei}^2 \Theta Z^{2/3} < 1$
RSB-1(2)	As SB-1(2), but with restriction of screening by R_0 (3)	As SB-1(2), but applicable at larger Γ_{ei}
LB-1(2)	LRT model with dynamical screening (39), (41) of Lenard-Balescu type, 1(2)-moment approach	As SB-1(2), but more accuracy near $\omega \approx \omega_{pl}$
GDW-1(2)	LRT model with account of electron-ion collisions by Gould-DeWitt (GDW) approximation (see [27]), 1(2)-moment approach (in the case of 2-moments approach, higher-moments correlation functions in renormalization factor r_ω are calculated by SB-2 model)	$\Gamma_{ei} \ll 1$; formal condition of applicability is $2.5\,\Gamma_{ei}^2 \Theta Z^{2/3} > 1$
LRT + PS_{EC}	Some of the LRT models listed above, using empty core pseudopotential as (64) with $r_{cut} = 0.4$ Å	
LRT + PS_R	Some of the LRT models listed above, using the pseudopotential by Rogers *et al.* [86]	
Pov + Λ	Semiempirical kinetic model by Povarnitsyn *et al.* [10] using different Coulomb logarithms Λ as listed below	$\omega \ll \omega_{pl}$, $Z \gg 1$ (electron -electron collisions are not accounted for)
Ner + Λ	Kinetic model (65) and (66) by Nersisyan *et al.*, which takes into account electron-electron collisions in degenerate plasmas, using different Coulomb logarithms Λ as listed below	$\Gamma_{ei} \ll 1$, $\omega \ll \omega_{pl}$
RNer + Λ	As Ner, but with effective collision frequency restricted by $\nu_{eff,max}$ (79) ($k_1 = 0.9$ for argon and xenon plasmas)	As for Ner
ΛSk-1/2(2/3)	Skupsky [35]-like model for Coulomb logarithm (80)–(83) with $C_{\Lambda,0} = 1/2(2/3)$, without screening by ions [with only the 1-st term under square root in (82)]	$\Gamma < 1$; DO correction for $\hbar\omega \ll T$—the term V_{th}/ω in (81)—is valid only for real part of Drude-like collision frequency ν_{Dr} (87)
ΛSk,i-1/2(2/3)	As ΛSk-1/2(2/3), but taking into account screening by ions [with all terms in (82)]	As for ΛSk-1/2(2/3)
ΛSt	Stygar *et al.* [34] model for the Coulomb logarithm (86)	$\Gamma_{ei} < 1$, $\omega \ll \omega_{pl}$, formal condition of applicability of the Born approximation used in the derivation is $2.5\,\Gamma_{ei}^2 \Theta Z^{2/3} > 1$
ΛERR	ERR fit formula for the Coulomb logarithm [68,70]	$\Gamma_{ei} < 1$, $Z = 1$, $\omega \ll \omega_{pl}$
Λp-2(3)	Velocity-dependent Coulomb logarithm (84) with 2 (3) terms in the right-hand side of (84)	$\Gamma_{ei} < 1$, $\omega \ll \omega_{pl}$
Λp,DO-2(3)	As Λp-2(3), but including DO correction, Eq. (85)	$\Gamma_{ei} < 1$, DO correction (85) for $\hbar\omega \ll T$ is valid only for real part of Drude-like collision frequency ν_{Dr} (87)
+ee	Including electron-electron collisions in LRT	
+Sii	Including ion correlations via a structure factor S_{ii} (62) in LRT models	Valid for estimation of the ion structure factor for noncrystalline materials, like liquid metals or dense plasmas

to be less than 1.5%. This accuracy can be further improved by increasing the accuracy of the integrals in the respective expressions for the correlation functions.

A. Brief summary of the models used in the calculations

For the readers' convenience we give here a brief summary of the models, described above and used below in particular calculations. In Table I the abbreviated designations of the models together with the references to the respective formulas and literature citations are given, as well as a note on the applicability. The abbreviated designations of the models in Table I have the form like "A", or "$A + B$", or "$C + \Lambda$", where "A" stands for the type of approximation within the LRT approach, "B" stands for the (pseudo)potential used, "C" gives an abbreviation for the the kinetic model, and "Λ" stands for the different models for the Coulomb logarithm, which are listed in the table as well. Unless stated otherwise (see the last lines in Table I), the electron-electron collisions and ion correlations in the form of a structure factor S_{ii} in LRT models are not accounted for.

B. Dependence of the DF on electron temperature

We investigate first the dependence of the DF $\varepsilon(\omega)$ on temperature. Additionally, we calculate the absorption coefficient $A = I_a/I_L$, where I_a and I_L are the flux densities absorbed in matter and incident from vacuum laser, respectively [87]. The absorption coefficient at normal incidence of laser radiation is related to the DF via $A = 4\,\mathrm{Re}\,\{\zeta\}/|1+\zeta|^2$ [90], with $\zeta = 1/\sqrt{\varepsilon}$ in the considered long-wavelength limit. As an example, we consider solid-density aluminum plasma with a constant average ion charge $Z = 3$ [91]. The plasma (with $T_\mathrm{i} = T$) is irradiated by a laser of wavelength $\lambda = 0.4$ nm. The laser frequency $\omega = 4.71 \times 10^{15}$ s^{-1} ($\hbar\omega = 3.09$ eV) is smaller than the plasma frequency $\omega_\mathrm{pl} = 23.9 \times 10^{15}$ s^{-1} ($\hbar\omega_\mathrm{pl} = 15.7$ eV), and therefore $\tilde{\omega} \ll 1$ is considered. The results of our comparative studies are shown in Figs. 1 and 2.

Figure 1 shows the real and imaginary part of the permittivity $\varepsilon(\omega)$ as well as the absorption coefficient A in dependence on the temperature considering different approximations. The plasma parameters Γ_ei, Γ_deg, and Θ are also given. For the frequency considered here, the LRT as described above gives practically identical results for the static (SB model) and dynamical (LB model) screening. The introduction of a minimum screening length in accordance with Eq. (45) leads to better agreement of the LRT with the semiempirical model by Povarnitsyn *et al.* [10], which was constructed using data of the reflectivity for laser-heated aluminum in the region of coupled plasmas.

Comparing the two graphs—SB-1 and SB-2—demonstrates that it is important to take into account higher moments of the electron distribution function. This can be done using a renormalization factor r_ω; see Ref. [19]. The one-moment approximation strongly overestimates the value of imaginary part of $\varepsilon(\omega)$.

Taking into account strong collisions via the Gould-DeWitt (GDW) model (see [27] for details of T-matrix and GDW calculations) and higher moments via the renormalization factor r_ω (GDW-2) leads to a good agreement for the absorption coefficient with the kinetic approximation for $\Gamma_\mathrm{ei} \leqslant 0.4$. Above temperatures of 100 eV, the effect of strong collisions (GDW-2) shows an effect of about 20% in the imaginary part of the permittivity in comparison to LB-2, SB-2, or RSB-2 models. The difference decreases with increasing temperature.

Using a pseudopotential of Rogers *et al.* [86] instead of a screened Coulomb potential, dynamical conductivity and absorption coefficient are strongly overestimated; see light green short-dashed curves SB-2 + PS_R compared with full circle SB-2 in Figs. 1(a)–1(c). It actually leads to an increase of the effective number of conducting electrons in comparison to the number of valence electrons, thus taking into account the influence of core electrons on the permittivity. Contrary to that, the empty core pseudopotential model [46] leads to an underestimation of the absorption in the considered case of aluminum plasmas; see dark green dashed curves SB-2 + PS_EC.

Figure 2 shows another set of calculations in order to compare LRT and kinetic models for the permittivity and the absorption coefficient. For some of the approaches, the effective collision frequency (74) is shown in (d). The semiempirical kinetic model of Povarnitsyn *et al.* [10] (see black dash-dotted

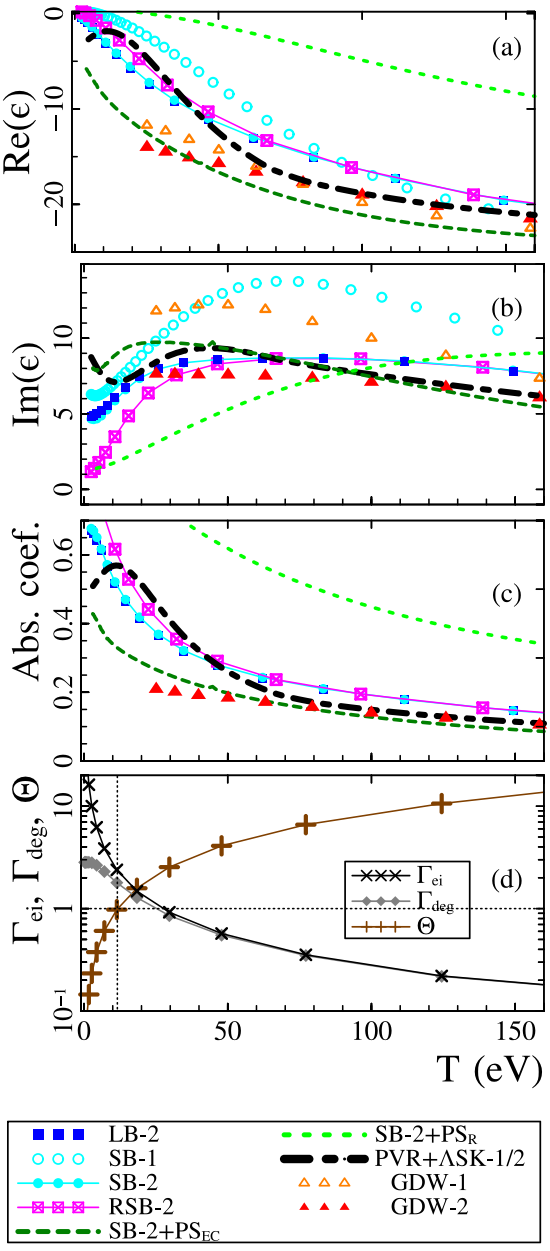

FIG. 1. Temperature dependence of the real (a) and the imaginary (b) part of the DF $\varepsilon(\omega)$ and the absorption coefficient A (c) at a frequency of 3.09 eV. The coupling parameters Γ_ei and Γ_deg and degeneracy parameter Θ are given in (d). The vertical dotted line denotes the Fermi energy. The models used are given in the legend; see Table I for explanations.

curves Pov+ΛSk-1/2) interpolates at $T \sim E_F$ between two different expressions: the phenomenological Drude formula for metallic plasma ($T < E_F$) and for $T > E_F$ and the integral formula for the ideal plasma permittivity of nondegenerate plasmas [24,25]. The two branches of the respective effective collision frequencies are shown in (d), the descending curve for the nondegenerate plasma ($T > E_F$) and the ascending curve for metallic plasmas. Calculations by Cauble and Rozmus [89] for a plasma with a steplike density profile are only shown for the absorption coefficient A at normal laser incidence; see brown curve with stars in Fig. 2(c). In the region of strongly

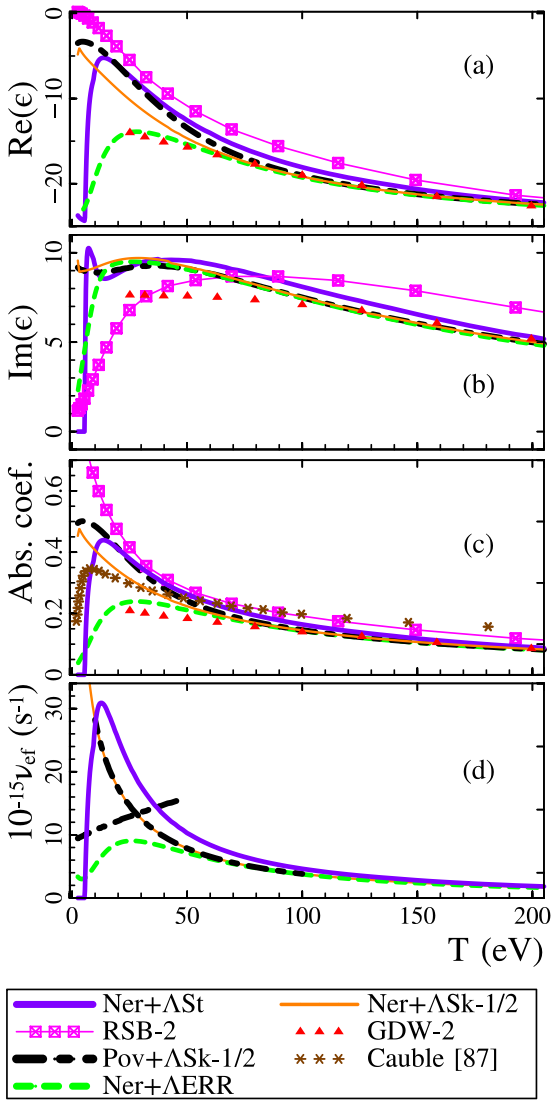

FIG. 2. The same as in Figs. 1(a)–1(c) and the electron-ion effective collision frequency $\nu_{\rm eff}$ (d) for a slightly extended temperature range. Not all models are shown again. Some additional models are added.

coupled plasmas (at temperatures $T \leqslant 50$ eV), their results considerably underestimate the absorption when comparing with the semi-empirical kinetic or LRT models. The ERR fit formula by Esser *et al.* [70] (green dashed curve Ner + ΛERR) and the Skupsky [35] model for the Coulomb logarithm Λ (thin orange solid curve Ner + ΛSk-1/2) also underestimate the absorption. The much lower absorption obtained by the Ner + ΛERR model at $T < 50$ eV is due to a lower Λ and consequently lower $\nu_{\rm eff}$, in comparison to the expressions given by Stygar *et al.* [34] (thick violet solid curves Ner + ΛSt) and in the Povarnitsyn *et al.* [10] model (dash-dotted black curves Pov + ΛSk-1/2). Note, that the validity of the ERR fit formula, which is based on numerical results of the LRT model and known limiting cases, does not extend to low temperatures.

On the other hand, for $T > 10$ eV, calculations using Stygar's interpolating expression for Λ (thick violet solid curves Ner + ΛSt) and the LRT model in the two-moment screened Born approximation (magenta curves with rectangular marks RSB-2) are in good agreement with the semiempirical model of Povarnitsyn *et al.* [10] (dash-dotted black curves Pov + Sk-1/2Λ). The latter is based on experimental data on the reflectivity of laser-heated aluminum. The ERR fit formula was originally derived for plasma with singly charged ions. This could be a reason why it underestimates slightly the dynamical conductivity for aluminum with $Z = 3$ at higher temperatures. The discrepancies at $T < 15$ eV are connected to the fact that electron-phonon interactions and absorption in metal-like plasmas, which lead to the ascending curve of absorption as a function of electron temperature and a maximum of absorption near $T = 15$ eV, are neither considered in the plasma LRT model described above or in the model of Nersisyan *et al.* for the permittivity [68] with Stygar's *et al.* [34] Coulomb logarithm. An approximate way to account for absorption in metal-like plasmas within the scope of the latter model is proposed in Ref. [76].

C. Frequency dependence of the dynamical collision frequency

The frequency dependence of the complex collision frequency $\nu_{\rm Dr} = \nu'_{\rm Dr} + i\nu''_{\rm Dr}$, defined in accordance with the generalized Drude formula (15) by

$$\begin{aligned} \nu'_{\rm Dr}(\omega) &= \omega\,{\rm Im}\,\{n/n_c/[1-\varepsilon(\omega)]\},\\ \nu''_{\rm Dr}(\omega) &= \omega\,{\rm Re}\,\{1-n/n_c/[1-\varepsilon(\omega)]\}, \end{aligned} \tag{87}$$

where $n_c = m\omega^2/(4\pi e^2)$ is the critical density, is shown in Figs. 3 and 4. Note that the value of $\nu_{\rm Dr}(\omega)$ defined by (87) is identical to the value $\nu(\omega)$ in LRT calculations (15) and (18), while for the KT calculations with the DF $\varepsilon(\omega)$ given by Eqs. (65) and (66), this complex value $\nu_{\rm Dr}(\omega)$ is quite different from the real value of the effective collision frequency $\nu_{\rm eff}$, though $\nu'_{\rm Dr}(\omega)$ is comparable to $\nu_{\rm eff}$; see Fig. 3.

From Fig. 3 it is seen that for an accurate description of the permittivity by the LRT approach, for frequencies lower than the plasma frequency, one needs to take into account not only the first, but also higher moments of the electron distribution function when calculating the correlation functions. For $\omega > \omega_{\rm pl}$ the first-moment approach is sufficient, i.e., $r_\omega \to 1$ for $\omega \gg \omega_{\rm pl}$.

It is also seen from Fig. 3 that at $\omega > 0.03\,\omega_{\rm pl}$ and especially at $\omega > 0.5\,\omega_{\rm pl}$ the imaginary part of $\nu_{\rm Dr}(\omega)$ is not well described by the kinetic model. This is due to the fact that the collisional term is independent on the frequency ω. On the contrary, the LRT model gives a consistent imaginary part of $\nu_{\rm Dr}(\omega)$ which satisfies the Kramers-Kronig relations, as discussed already above.

Figure 4 demonstrates a comparison of the LRT and different kinetic models using different expressions for the Coulomb logarithm, however taking the same parameters as in Fig. 3. For the temperature $T = T_{\rm i} = 300$ eV the plasma is nondegenerate ($\Theta = 26$) and weakly coupled ($\Gamma_{\rm ei} = 0.091$). For the average ion charge $Z = 3$, the influence of electron-electron collisions is not significant. Therefore, the results using the expression for $\varepsilon(\omega)$ according to the Povarnitsyn *et al.* semiempirical kinetic model [10] and to the Nersisyan *et al.* model [68] for plasmas with arbitrary Z and similar

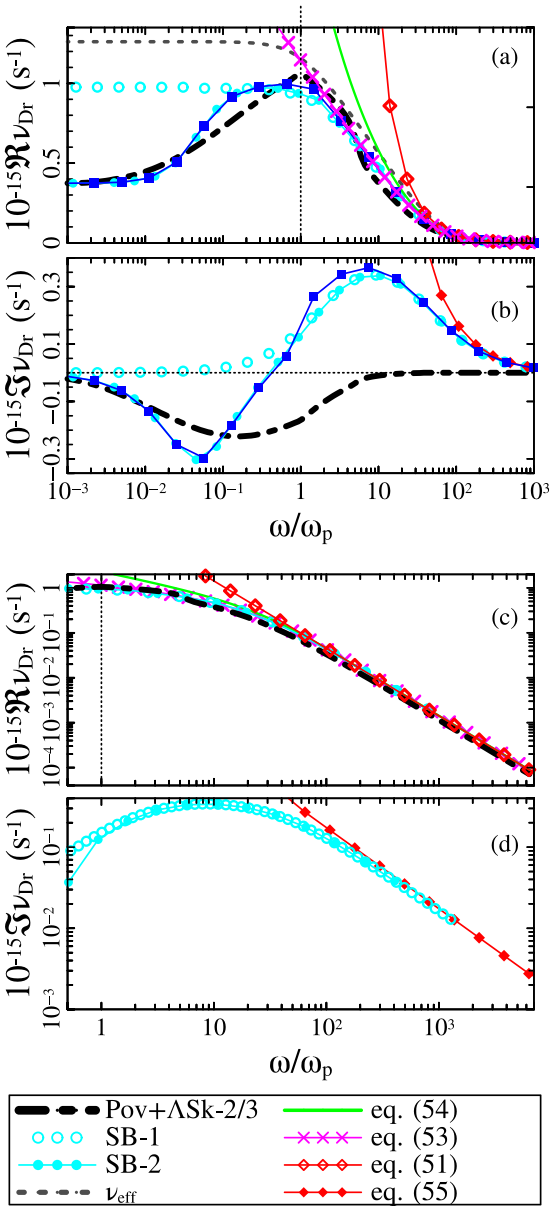

FIG. 3. Real (a),(c) and imaginary (b),(d) parts of the generalized Drude-like collision frequency $\nu_{Dr}(\omega)$ (87) as function of the laser frequency radiating solid-density aluminum plasma at $T_i = T = 300$ eV considered in different frequency ranges. The models used are given in the legend; see Table I for explanations and asymptotic formulas in Sec. II E.

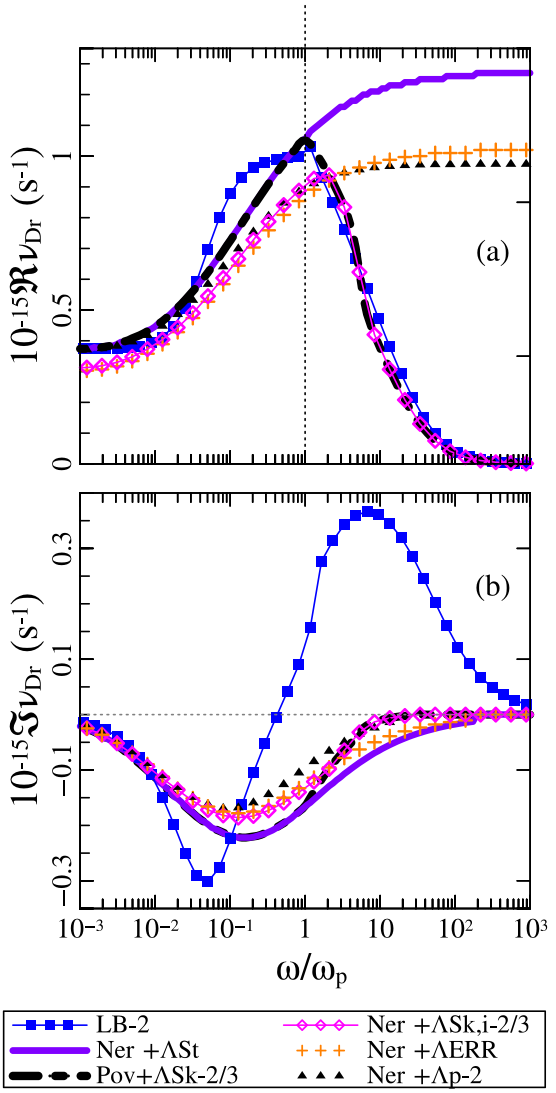

FIG. 4. The same as in Fig. 3. The models used are different and given in the legend; see Table I for explanations.

models for Lorentz plasmas [73] are very close; differences arise from different forms of the Coulomb logarithm.

It is seen from Fig. 4 that, for plasma parameters considered here, the second Born approximation for Λ as used by Stygar *et al.* [Eq. (86) and Ref. [34]; see violet solid curves Ner + ΛSt] almost coincides with the Skupsky-like model (80)–(83) (see black dash-dotted curve Pov + ΛSk-2/3) for moderate frequencies $\omega < \omega_{pl}$. Furthermore, the expression (84) without the contribution of ion correlations [i.e., with only two terms on the right hand side of Eq. (84)], see black triangular marks Ner + Λp-2, gives also very similar results for small laser frequencies $\omega < 0.1\ \omega_{pl}$.

Still considering Fig. 4, the model (80)–(83), graph Pov + ΛSk-2/3, is in good agreement with the LRT for $\nu'_{Dr}(\omega)$, graph LB-2, in the entire frequency range. The account of screening by ions slightly decreases the value of $\nu'_{Dr}(\omega)$; see the graphs Ner + ΛSk,i-2/3 with the diamond markers. Very similar results are obtained by the ERR fit formula for Λ [68,70] (see the graphs Ner + ΛERR), at moderate laser frequencies and temperature considered in this figure.

Figure 5 demonstrates the effect of different screening and ion correlations for moderately coupled ($\Gamma_{ei} \sim 1$) solid-density, partially degenerated aluminum plasmas at temperature $T_i = T = 20$ eV. For the coupled plasmas considered here, the restriction of the screening radius from below by R_0 (3) substantially influences the value of $\nu_{Dr}(\omega)$, especially in the region $\omega \in (0.4 - 2)\ \omega_{pl}$. The real part as well as $|\nu''_{Dr}(\omega)|$ are considerably increased. The account of ion correlations through S_{ii} also substantially influence the value of $\nu_{Dr}(\omega)$, leading to a decreasing peak near $\omega = \omega_{pl}$. As already stated, for the ion charge $Z = 3$ considered here, the influence of e-e collisions on the dynamical collision frequency is marginal.

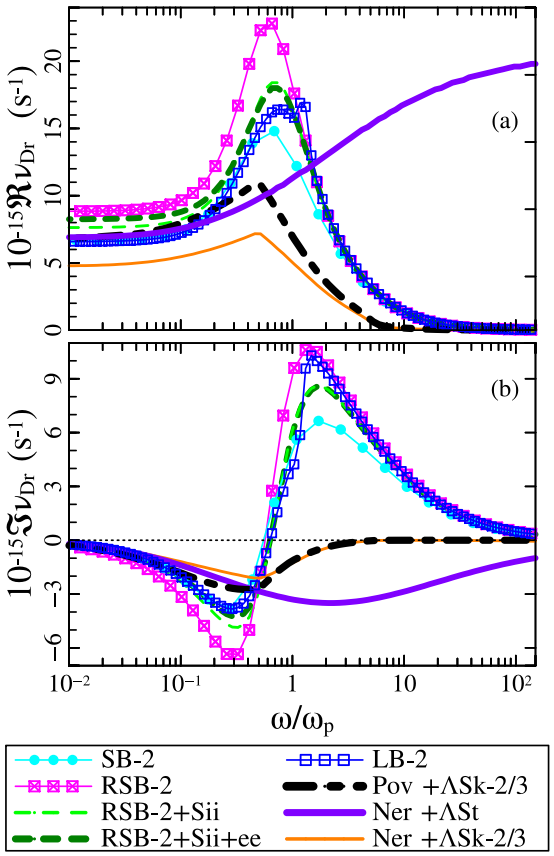

FIG. 5. Real and imaginary parts of the generalized Drude-like collision frequency $\nu_{Dr}(\omega)$ (87), as functions of the laser frequency radiating solid-density aluminum plasma at $T_i = T = 20$ eV. The models used are given in the legend; see Table I for explanations.

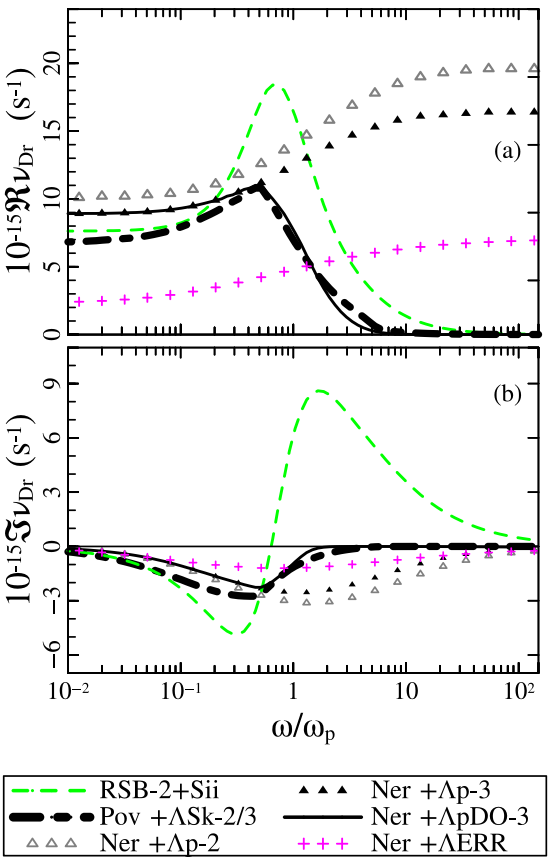

FIG. 6. The same as in Fig. 5. The models used are different and given in the legend; see Table I for explanations.

Unlike the case of weakly coupled plasmas (Fig. 3), it is seen from Fig. 5 that for moderately coupled plasmas the agreement between LRT and kinetic calculations can be observed only for relatively small frequencies $\omega \lesssim 0.3\ \omega_{pl}$. For higher frequencies, all kinetic models underestimate the value of $|\nu_{Dr}(\omega)|$.

Figure 6 complements Fig. 5. Additionally it shows calculations with various options for the Coulomb logarithm (84) and the ERR Coulomb logarithm [68,70]. The account of the third term in Eq. (84), responsible for the ion correlations [80], improves the correspondence with LRT results for $\omega \lesssim 0.3\ \omega_{pl}$. However, the discrepancies at higher frequencies between both approaches are not removed. Using the ERR fit formula for Λ underestimates $|\nu_{Dr}(\omega)|$ in the entire frequency range for the coupled plasmas considered here, which, as already stated, can be related to the fact that originally this model was formulated for plasmas with singly charged ions.

D. Comparison with experimental data

An interesting experimental quantity is the dc conductivity $\sigma_{dc} = \sigma(\omega \to 0)$. It is here considered as the dimensionless quantity

$$\sigma^* = \frac{Z\sqrt{m}e^2}{T^{3/2}}\sigma_{dc} = \frac{3}{4\sqrt{2\pi}}\Lambda_{dc}^{-1}, \tag{88}$$

which is basically proportional to the inverse of the Coulomb logarithm Λ_{dc}.

Figure 7 shows σ^* at a fixed temperature of about 25 000 K as a function of the coupling parameter Γ_{ei}. For direct comparison with experiments, in this section the temperatures are given in units of K. Several theoretical approaches presented in this paper are compared with experimental data obtained from rare gas plasmas argon and xenon. Both LRT and kinetic approaches describe the experimental data points reasonably well, if one takes into account the restriction (79) of the maximum of the effective collision frequency as well as electron-electron collisions. In addition, results are shown taking into account simultaneously both the ion correlations through S_{ii}, the restriction of the screening radius through R_0 (3), and the effect of the interaction of the conducting electrons with inner core electrons through a pseudopotential [see Eq. (63)] with radius $r_{cut} = 0.5$ Å. The LRT screened Born calculations, with account of S_{ii} only, give also satisfying agreement with the experimental data points.

Figure 8 shows the reflectivity $R = 1 - A$, which was obtained from shock wave experiments on Xe plasmas at different free electron densities n_e. In the experiment in [94] the thermodynamic parameters of the plasma were determined from the measured shock wave velocity. The plasma composition, in particular n_e, was calculated within the chemical model [95]. At the considered temperatures, only

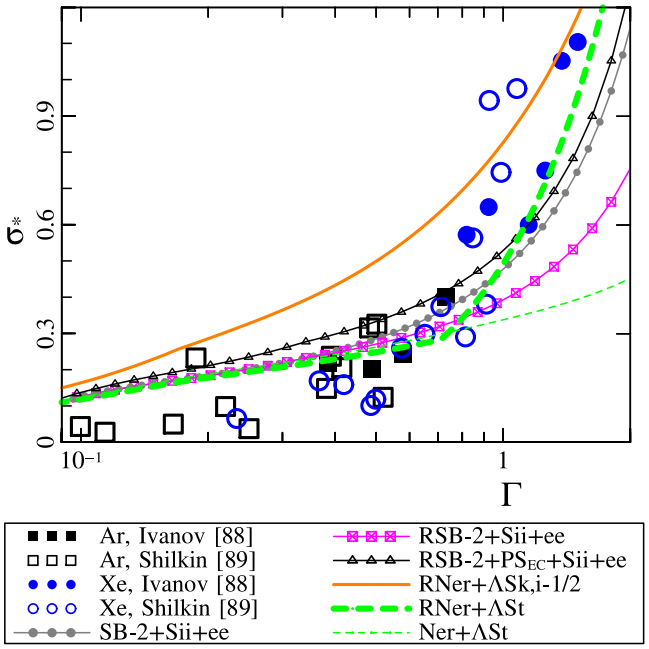

FIG. 7. Dimensionless dc conductivity σ^* [Eq. (88)] as a function of the coupling parameter Γ_{ei} for dense argon and xenon plasmas at temperature $T = T_i \approx 25\,000$ K. Experimental points of Ivanov *et al.* [92] and Shilkin *et al.* [93] for xenon and argon plasmas are shown by large markers and calculations using LRT and KT models are depicted by (marked) lines; see legend and Table I for explanations.

singly charged ions are present; therefore, we used $Z = 1$ in the calculations.

Calculations by the LRT model with and without the restriction of the screening radius from below by R_0 are shown in Fig. 8. It can be seen that the calculations taking into account the restriction of screening in strongly coupled plasmas are

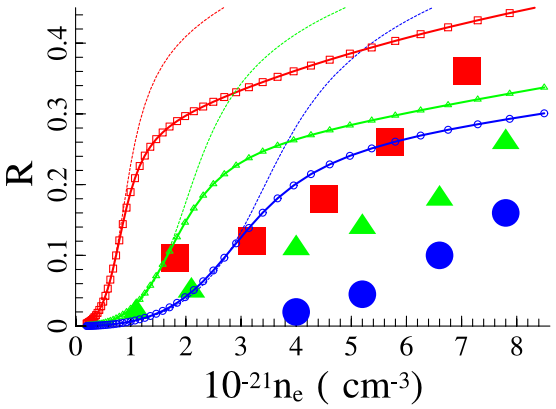

FIG. 8. Reflectivity R as a function of the free electron density n_e obtained from shock wave experiments on xenon plasmas, $T = T_i \approx 30\,000$ K. Experimental data [94] are shown by large markers: red squares for wavelength $\lambda = 1.06$ μm; green triangles for $\lambda = 0.694$ μm; blue circles for $\lambda = 0.532$ μm. Marked lines (with the same colors and markers for the same λ) show the LRT calculations (model RSB-2 + PS_{EC} + ee); dotted lines show the same, but without the restriction of the screening radius from below by R_0 (model SB-2 + PS_{EC} + ee).

closer to the experimental points, though still the results are above the experimentally measured reflectivity.

Note that the plasma density profile of the shock front was assumed to be steplike. Previous studies had shown that a finite width of the shock wave front [96–99] and the contribution of transitions of electrons from bound shells [100] influence substantially the reflectivity. The account of those effects can improve significantly the correspondence of theoretical and experimental results. The contribution of bound-bound transitions and the role of plasma inhomogeneities are investigated in the following section.

V. ESTIMATION OF CONTRIBUTIONS DUE TO BOUND-BOUND TRANSITIONS AND PLASMA INHOMOGENEITIES

A. Role of plasma inhomogeneities

Shock waves have a final width L_S at its front where plasma parameters (for instance, temperature, pressure, ion concentration, and ionization degree) smoothly change from their upstream (nonperturbed) values T_0, P_0, $n_{i,0}$ to their downstream values T_1, P_1, $n_{i,1}$.

Estimates on the basis of kinetic equations [101] or the Boltzmann H theorem [102] give a value for the width of the shock wave front of the order of the mean free path of atoms or molecules in the nonperturbed gas. Thus, one can write

$$L_S \approx C_{L_S}/(n_{i,0}\sigma_c), \tag{89}$$

where C_{L_S} is a constant and σ_c is the cross section of atomic collisions. The upstream heavy particle density $n_{i,0}$ is related to the downstream heavy particle density $n_{i,1}$ by Rankine-Hugoniot expressions. For strong shock waves (Mach number $M \gg 1$) in a polytropic gas [101,103] it is found that

$$n_{i,1} = n_{i,0}(\gamma + 1)/(\gamma - 1), \tag{90}$$

where γ is the adiabatic coefficient of the gas.

The influence of the plasma inhomogeneity, owing to the finite width of the shock wave front, on laser radiation absorption in the plasma depends on the ratio $\kappa_S = L_S/l_s$, where l_s is the plasma skin layer depth. From the solution of the wave equation for a uniform plasma with steplike density profile, the permittivity (15), and $\omega < \omega_{pl}$, one can write an expression for l_s,

$$l_s \approx \frac{c}{\omega_{pl}} \frac{\sqrt{1+\breve{\nu}^2}}{\sqrt{1-(\omega/\omega_{pl})^2(1+\breve{\nu}^2)}} \approx \frac{c}{\omega_{pl}}, \tag{91}$$

where $\breve{\nu} = \mathrm{Re}\{\nu(\omega)\}/\omega$. The second approximate equality is valid for the case $\breve{\nu} \ll 1$ and $\omega_{pl} \gg \omega$.

From Eqs. (89)–(91) one has the following expression for the ratio κ_S defined above:

$$\kappa_S \approx C_{L_S} \frac{\gamma+1}{\gamma-1} \frac{2\sqrt{\pi Z}e}{\sqrt{mc}\sqrt{n_{i,1}}\sigma_c} \approx 6\times 10^{-2} C_{L_S} \frac{\gamma+1}{\gamma-1} \times \left[\frac{Z}{n_{i,1}/10^{21}\ \mathrm{cm}^{-3}}\right]^{1/2} \left[\frac{\sigma_c}{10^{-15}\ \mathrm{cm}^2}\right]^{-1}. \tag{92}$$

Numerical calculations on the basis of the solution of the Navier-Stokes equations give a parameter value $C_{L_S} \approx 4$ for shock waves with Mach numbers M of several units in

argon; see Refs. [104,105]. Similar results for C_{L_S} follow from the numerical solution of the Burnett equations obtained in Ref. [106]. Simulations on the basis of the solution of the Boltzmann kinetic equations indicate even higher values, $C_{L_S} \approx 10$ [107].

The value of σ_c can be estimated using a fitting formula proposed in Ref. [108] for the total elastic cross section of argon on argon atoms with the relative energy E,

$$\sigma_c \approx 2.1\left(\frac{E}{\text{eV}}\right)^{-0.4}\left[1+\left(\frac{E}{15\text{ eV}}\right)^2\right]^{0.16} \times 10^{-14}\text{ cm}^2, \tag{93}$$

which gives the value $\sigma_c \sim 10^{-14}$ cm^2 for the average relative energy $E \approx 3$ eV. Substituting this value and the values $Z = 1$, $C_{L_S} = 4$, and $\gamma = 5/3$ into Eq. (92), one obtains the following estimate for the experimental conditions relevant for Fig. 8:

$$\kappa_S \sim 0.1(n_{\text{i},1}/10^{21}\text{ cm}^{-3})^{-1/2}. \tag{94}$$

In order to elucidate the influence of the parameter κ_S on the absorption of laser energy, let us consider a plasma density profile with a linear ramp: $n_\text{i}(x) = 0$ for $x < 0$, $n_\text{i}(x) = \text{const} = n_{\text{i},1}$ for $x > L_S$, $n_\text{i}(x) = n_{\text{i},1}x/L_S$ for $0 < x < L_S$ (the plasma temperature is assumed to be constant). Under the assumption of weak absorption (with $|\nu(\omega)|/\omega \ll 1$) and for overcritical plasma density ($\omega_\text{pl} \gg \omega$) one can express the solution of the wave equation for such a plasma profile in terms of the Airy functions Ai and Bi of the first and the second kind, respectively. Then the change of the absorption coefficient (see Ref. [109]) $\alpha = A/A_\text{st}$, given by the ratio of the real absorption coefficient A for a given plasma profile to the absorption coefficient A_st for a plasma with steplike density profile [$n_\text{i}(x) = \text{const} = n_{\text{i},1}$ for $x > 0$, and $= 0$ else], can be expressed as

$$\begin{aligned}
\alpha &= \frac{\frac{\omega_\text{pl}^2}{\omega^2}\left[1+\frac{2}{\kappa_S}\int_{-L_0}^{L_1}\Phi^2(x)(x+L_0)^2\,dx\right]}{\Phi^2(-L_0)+\Phi'^2(-L_0)/L_0},\\
\Phi(x) &\equiv C_1\,\text{Ai}(x) - C_2\,\text{Bi}(x),\\
C_1 &= \frac{\kappa_S^{1/3}\,\text{Bi}(L_1)+\text{Bi}'(L_1)}{\text{Ai}(L_1)\,\text{Bi}'(L_1)-\text{Bi}(L_1)\,\text{Ai}'(L_1)},\\
C_2 &= \frac{\kappa_S^{1/3}\,\text{Ai}(L_1)+\text{Ai}'(L_1)}{\text{Ai}(L_1)\,\text{Bi}'(L_1)-\text{Bi}(L_1)\,\text{Ai}'(L_1)},\\
L_0 &= (\omega/\omega_\text{pl})^2\kappa_S^{2/3}, \quad L_1 = [1-(\omega/\omega_\text{pl})^2]\kappa_S^{2/3},
\end{aligned} \tag{95}$$

with $\Phi'(L_0) \equiv \partial\Phi(x)/\partial x|_{x=L_0}$, and similarly for $\text{Ai}'(L_1)$.

From Eq. (95) it follows that, in the limit of weak absorption, the function α is independent on the absorption mechanism [i.e., of $\nu(\omega)$] and depends on two variables only: L_0 and ω_pl/ω. For $\kappa_S \to 0$ we have $\alpha \to 1$, and for $\kappa_S \gg 1$ the second term in Eq. (95) exceeds the first one, 1. The function $\Phi(x)$ is of the order of $\text{Ai}(x)$, and the function α is mainly dependent on L_0. From that follows that the lower the ratio $n/n_c = (\omega_\text{pl}/\omega)^2$ of the maximum plasma density to the critical density n_c, the higher is the influence of a finite width L_S of the plasma density ramp on the absorption.

The behavior of $\alpha(\kappa_S)$ for different wavelengths corresponding to the experimental ones (see Fig. 8) and different

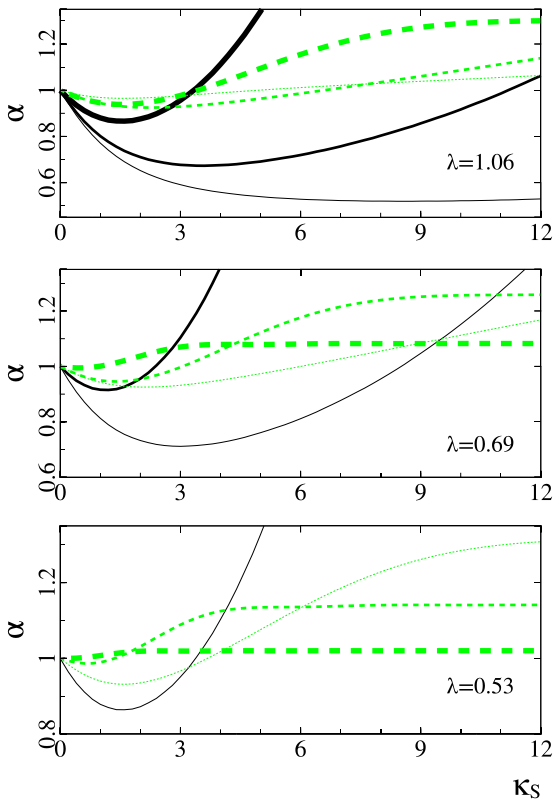

FIG. 9. Ratio $\alpha = A/A_\text{st}$ as function of ratio $\kappa_S = L_S/l_s$ of a plasma with linear ramp of its density profile for different wavelengths λ in μm. Different electron densities are considered: $n = 1.5,\ 3,\ 6 \times 10^{21}$ cm^{-3} for thick, medium, and thin curves, respectively. The calculations in the limit of weak plasma absorption by formula (95) are shown by solid curves, but only as long as $n/n_c > 1$. Numerical calculations with absorption determined by the three-moment screened Born approximation for xenon plasmas with $T = T_\text{i} = 30\,000$ K are shown by dashed curves.

electron densities is shown in Fig. 9. Curves are presented which are calculated using the expression (95) in the limit of weak absorption as well as curves calculated by the numerical solution of the wave equation for a plasma with permittivity given by Eqs. (15), (18), (19), (B5), (B6), and (B7) (two-moment screened Born approximation with account of the contribution of electron-electron collisions).

For the plasma parameters considered here, we have $|\nu(\omega)/\omega| \gtrsim 1$. This is the reason why the calculations shown by dashed lines in Fig. 9 deviate from the analytical estimates based on Eq. (95). In particular, a saturation of the increase of absorption with increasing κ_S is seen for κ_S exceeding some value $\kappa_S = \kappa_{S^*}$. Nevertheless, the above mentioned conclusion about the increasing influence of κ_S on absorption with a decreasing ratio n/n_c remains true. From Fig. 9 one can see that the critical ratio κ_{S*} is decreasing with shorter wavelengths and (or) the diminishment of the plasma density. Particularly, $\kappa_{S^*} \approx 1.5,\ 4,\ 12$ for $n = 1.5,\ 3,\ 6 \times 10^{21}$ cm^{-3}, respectively, and $\lambda = 0.53$ μm; $\kappa_{S^*} \approx 3,\ 9$ for $n = 1.5,\ 3 \times 10^{21}$ cm^{-3}, respectively, and $\lambda = 0.69$ μm; $\kappa_{S^*} \approx 12$ for $n = 1.5 \times 10^{21}$ cm^{-3} and $\lambda = 1.06$ μm. Under the assumption of a finite width of the shock wave front, this could explain why the discrepancy between experimental results and theoretical calculations in

Fig. 8, performed with the assumption $\kappa_S = 0$, is larger for lower plasma densities and for shorter wavelength. Also, the dependence of the experimentally determined reflectivity on the electron density shows concave curves, while the theoretical calculations under the assumption of $\kappa_S = 0$ leads to convex ones.

One can see from Fig. 9 that a pronounced effect of a nonzero κ_S on the increase of plasma absorption can be achieved only for $\kappa_S \gtrsim 3$, while theoretical estimates of the width of the shock wave front (94) gives about 30 times lower values of $\kappa_S \lesssim 0.1$ for $n_i \geqslant 10^{21}$ cm^{-3}.

From the above consideration follows that an increased absorption or a decreased reflectivity of laser radiation from the shock wave front, in comparison with theoretical predictions for $L_s = 0$, could be a signature of a considerable broadening of the width of the shock wave front due to ionization or excitation processes [101,103]. Consequently, such increased absorption could serve as a diagnostic tool to analyze nonstationary processes at the shock wave front.

B. Estimates for the contributions of interband transitions

Recently, numerical calculations of the reflectivity of shock compressed argon and xenon plasmas utilizing the density functional approach and the Kubo-Greenwood (KG) formula have been performed. They have shown that interband transitions play an essential role and should be accounted for when interpreting the respective experimental results [100,110]. Below, a semiphenomenological estimate of this effect is given.

One can note that taking into account interband transition effects corresponds to the inclusion of collisions with bound states in particular atoms. These should be considered in addition to electron collisions with free charge carriers; see [111].

With the account of interband transitions, the permittivity can be expressed as

$$\varepsilon(\omega) = \varepsilon_{\mathrm{Dr}}(\omega) + \delta\varepsilon_{\mathrm{b}}(\omega), \tag{96}$$

where $\varepsilon_{\mathrm{Dr}}(\omega)$ is the intraband or Drude-like contribution to the permittivity, given by (15), and $\delta\varepsilon_{\mathrm{b}}(\omega)$ is the interband contribution to the permittivity.

Different approaches can be used to determine $\delta\varepsilon_{\mathrm{b}}(\omega)$: Besides first-principles calculations using the KG formula (see Ref. [100,112]) and their modifications on the basis of the average-atom model [48], the Drude-Lorentz (DL) model [113–116] and its modification in the form of the critical points model [116,117] are widely used for the approximate description of interband contributions to the permittivity. In this way, semiempirical interpolation formulas for the optical properties of a wide class of substances (metals, dielectrics, amorphous materials) are obtained.

The DL model for $\delta\varepsilon_{\mathrm{b}}(\omega)$ can be rewritten in the form

$$\delta\varepsilon_{\mathrm{b}}(\omega) = -\omega_{\mathrm{pl},n_i}^2 \sum_{m,n} \frac{F_{mn}^x}{\omega^2 - \omega_{mn}^2 + i\omega\Gamma} f_{\mathrm{F}}(E_n)[1 - f_{\mathrm{F}}(E_m)], \tag{97}$$

where we introduced Γ as a damping factor, $\omega_{mn} = (E_m - E_n)/\hbar$, and $\omega_{\mathrm{pl},n_i}^2 = 4\pi n_i e^2/m$. E_m is the energy of the mth energy level (or energy of a continuum state in the case of bound-free transitions). The matrix element $F_{mn}^x = 2\,m\,\omega_{mn}|\langle m|x|n\rangle|^2/\hbar$ is the oscillator strength [118] and $f_{\mathrm{F}}(E) = \{1 + \exp[(E-\mu)/T]\}^{-1}$ the Fermi function. The sum in (97) is to be taken over all permitted dipole transitions, with $l_m = l_n \pm 1$, where $l_{m,n}$ are the respective orbital quantum numbers.

Unlike the usual DL model, Eq. (97) contains the factor $f_{F_{mn}} \equiv f_{\mathrm{F}}(E_n)[1 - f_{\mathrm{F}}(E_m)]$ which accounts for the population of the energy levels and the Pauli blocking principle. For $\Gamma \to 0$ the imaginary part of Eq. (97) represents a sum of δ functions $\delta(\omega + \omega_{mn}) + \delta(\omega - \omega_{mn})$. In this case, similarly to that shown in Ref. [119], one can derive from Eq. (97) an expression for the imaginary part of $\delta\varepsilon_{\mathrm{b}}(\omega)$ which is equivalent to the KG formula.

In the case of laser radiation frequencies much below the transition frequencies, $\omega \ll |\omega_{mn}|$ (which is the case for the reflectivity measurements depicted at Fig. 8), and for $\Gamma/\omega \ll 1$, the contribution to the imaginary part of $\delta\varepsilon_{\mathrm{b}}(\omega)$ is close to 0. The main contribution of the interband transitions on the reflectivity (or absorption) comes from $\mathrm{Re}\,\{\delta\varepsilon_{\mathrm{b}}(\omega)\}$. In accordance with Eq. (97), the contribution of the jth interband transition to $\mathrm{Re}\,\{\delta\varepsilon_{\mathrm{b}}(\omega)\}$ is proportional to

$$\delta\varepsilon'_{\mathrm{b},j}(\omega) = \left(\frac{\omega_{\mathrm{pl},n_i}}{\omega_{mn,j}}\right)^2 F_{mn,j}^x f_{F_{mn,j}} \left[1 - \frac{\omega^2}{\omega_{mn,j}^2}\right]^{-1}. \tag{98}$$

For $\omega \ll |\omega_{mn}|$ the contribution (98) depends only weakly on the frequency ω. However, it can be dependent on the plasma density n_i via the expressions for ω_{pl,n_i}, ω_{mn}, and $f_{F_{mn}}$. One can assume that ω_{mn} and $f_{F_{mn}}$ are slowly dependent on n_i in comparison to $\omega_{\mathrm{pl},n_i}^2 \sim n_i$. Otherwise, the increase of the energy gap ΔE_{bf} between bound pair excited states (with energies $E_n < 0$) and free states of electron gas (with energies $E_f > 0$) is approximately proportional to $n_i^{1/3}$,

$$\Delta E_{bf} \approx 4.6\ \mathrm{eV}\ Z(n_i/10^{21}\ \mathrm{cm}^{-3})^{1/3}; \tag{99}$$

see Refs. [120,121].

Since only states with energies $E_n < -\Delta E_{bf}$ can contribute to interband transitions, the number of transitions contributing to $\delta\varepsilon_{\mathrm{b}}(\omega)$ decreases with increasing plasma density,

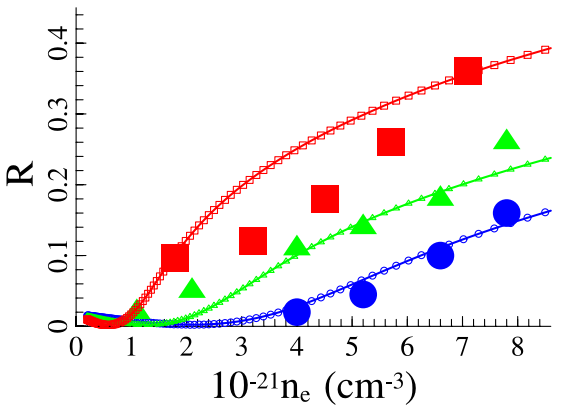

FIG. 10. The same as in Fig. 8, but with the account of a nonzero value of $\mathrm{Re}\,\{\delta\varepsilon_{\mathrm{b}}(\omega)\}$ in the calculations (solid marked lines). A constant value $\mathrm{Re}\,\{\delta\varepsilon_{\mathrm{b}}(\omega)\} = 0.7$ was used in all calculations.

in accordance with (99). Keeping in mind that transitions from the upper excited levels can give the main contribution to the interband absorption (see, e.g., Ref. [48]), such a decrease can be rather essential and could compensate the linear increase of $\omega^2_{\mathrm{pl},n_i}$ with n_i.

Figure 10 illustrates that the simplest assumption of a constant value independent on density, $\mathrm{Re}\,\{\delta\varepsilon_b(\omega)\} \approx 0.7$ [122], leads to a considerably better agreement between the experimental results and the calculations. For the considered plasma and laser radiation parameters, the value of $\omega_{\mathrm{pl}}/\omega > 1$ is not far from 1 and hence $\mathrm{Re}\,\{\varepsilon(\omega)\} < 0$ for $n_i > 10^{21}$ cm^{-3}. The addition of a small positive nonzero value for $\mathrm{Re}\,\{\delta\varepsilon_b(\omega)\}$ brings $\mathrm{Re}\,\{\varepsilon(\omega)\}$ closer to zero, thus making the plasma more transparent for laser radiation.

VI. CONCLUSIONS

The LRT model has been used to develop a model for the intraband part of the permittivity in WDM. It is suitable in a wide frequency range, from the far infrared including the dc limit to the x-ray region. The model accounts for both electron-ion and electron-electron collisions, arbitrary degeneracy, screening, and correlation effects. The relevant formulas are (15), (18), (19), (B3)–(B7), (39), (41), and (45)–(48). Approximate expressions have been derived as simple fits, which enables us to use them in hydrodynamic codes.

It is shown that the approach elaborated from the LRT is in good agreement with different versions of the kinetic model derived from the Boltzmann kinetic equation if higher order moments of the electron distribution function are taken into account. This holds for low frequencies ($\omega < \omega_{\mathrm{pl}}$) and for moderate coupling.

At high frequencies ($\omega > \omega_{\mathrm{pl}}$), the introduction of Dawson-Oberman-like corrections into classical kinetic models ensures a good agreement of the real part of the Drude-like effective collision frequency ν_{Dr} (87), obtained within KT, with the results of LRT calculations. Nevertheless, the imaginary part of ν_{Dr} is not correctly described by this correction procedure within the classical kinetic approach, and the LRT model should be used for the calculation of $\mathrm{Im}\,\{\nu_{\mathrm{Dr}}\}$ in this frequency range. In addition, LRT gives a proper description of the inverse bremsstrahlung absorption of high-frequency laser radiation.

Simple expressions are obtained from the LRT approach in the region of low coupling where the Born approximation can be applied. Strong collisions are included within the Gould-DeWitt scheme results. The real and the imaginary parts of permittivity calculated by the LRT model for optical frequencies and weak or moderate coupling are almost identical with those obtained within the kinetic approach.

Effects of screening are studied and it is shown that statical screening of the interaction potential gives the same results as obtained from dynamical screening at all frequencies except the region of the plasmon resonance in the vicinity of $\omega = \omega_{\mathrm{pl}}$. In the region of strong coupling, the limitation of the screening length by the interatomic distance is necessary for the correct description of optical properties of matter. Furthermore, ion correlations should be taken into account in the region of moderate and strong coupling for the accurate description of permittivity.

As an application of the theory for calculating the DF, optical properties of shock compressed noble gas plasmas have been considered. In addition to the contribution of free electrons (intraband contribution), also the contribution of bound electrons (inter band contribution) to the permittivity and the final width L_S of the shock wave front must be taken into account. Furthermore, it was shown that for the considered plasma densities and wavelengths, a final width $L_S \gtrsim 3l_s$, where l_s is the skin layer depth, can lead to a considerable increase of the absorption coefficient A. In this way, a change of the shape of the reflectivity curve $R(n)$ in dependence on the free electron density n from initially convex to a more concave one is possible. This behavior is closer to the results seen in experiments. On the other hand, such values of L_S are about 30 times larger than estimates made for the equilibrium shock wave front width, determined by ion-ion collisions [101,102]. Therefore, for a more precise estimate of the width of a shock wave front, it is necessary to take into account relaxation processes, ionization, and excitation. Our approach shows the possibility to use optical measurements of the reflectivity of shock compressed gases as a tool for the diagnostics of the structure of the shock wave front and relaxation processes in it.

ACKNOWLEDGMENTS

We are grateful to N. E. Andreev for valuable discussions. M.V. thanks his German colleagues for hospitality and financial support during his visits to Rostock University and Johannes Kepler University in Linz. The work of M.V. in JIHT was partly supported by the Presidium of RAS program "Thermo-physics of High Energy Density," Grant No. I.13P. The authors acknowledge financial support by collaborative projects funded jointly by RAS and Deutsche Forschungsgemeinschaft (Germany). Furthermore, H.R. and G.R. acknowledge support within the Deutsche Forschungsgemeinschaft (Germany) funded Special Research Unit, Grant No. SFB 652.

APPENDIX A: GENERALIZED LINEAR RESPONSE THEORY

According to [19] (see also [18,20,43]), the nonequilibrium statistical operator $\hat{\rho}(t)$ is determined by the dynamical evolution of the system with Hamiltonian $\hat{H}_{\mathrm{tot}} = \hat{H} + \hat{H}_{\mathrm{ext}}(t)$,

$$\hat{\rho}(t) = \lim_{\delta\to+0} \delta \int_{-\infty}^{t} dt' e^{-\delta(t-t')} \hat{U}(t,t') \hat{\rho}_{\mathrm{rel}}(t') \hat{U}^{\dagger}(t,t'), \quad \text{(A1)}$$

where $\hat{U}(t,t')$ is the time evolution operator, which solves the equation $i\hbar\partial_t \hat{U}(t,t') = \hat{H}_{\mathrm{tot}}\hat{U}(t,t')$ with initial condition $\hat{U}(t',t') = 1$. The system Hamiltonian $\hat{H}$ is determined by Eq. (1). The external perturbation $\hat{H}_{\mathrm{ext}}(t)$ is determined in dipole approximation as

$$\hat{H}_{\mathrm{ext}}(t) = -e\hat{\boldsymbol{R}} \cdot \boldsymbol{E}(t), \ \hat{\boldsymbol{R}} = \sum\nolimits_i \hat{\boldsymbol{r}}_i, \quad \hat{\dot{\boldsymbol{R}}} = \hat{\boldsymbol{P}}_{0,1}/m, \quad \text{(A2)}$$

where $\hat{\boldsymbol{P}}_{0,1}$ is defined by Eq. (11).

$\hat{\rho}_{\rm rel}(t)$ is the relevant statistical operator. It is introduced as a generalized Gibbs ensemble, which is derived from the principle of maximum of entropy,

$$\hat{\rho}_{\rm rel}(t) = Z_{\rm rel}(t)^{-1} \exp\left[-\beta(\hat{H} - \mu\hat{N}) + \sum_n F_n(t)\hat{B}_n\right],$$
$$Z_{\rm rel}(t) = {\rm Tr}\exp\left[-\beta(\hat{H} - \mu\hat{N}) + \sum_n F_n(t)\hat{B}_n\right], \qquad \text{(A3)}$$

where the Lagrange parameters β, μ, and $F_n(t)$ are introduced to fix the given averages,

$${\rm Tr}\{\hat{B}_n\rho(t)\} = \langle\hat{B}_n^t\rangle = {\rm Tr}\{\hat{B}_n\rho_{\rm rel}(t)\}, \qquad \text{(A4)}$$

and similar equations holds for determination of β and μ from conditions on $\langle\hat{H}\rangle$ and $\langle\hat{N}\rangle$, where $\hat{N} = \sum_p \hat{a}_p^\dagger\hat{a}_p$. Equation (A1) means that further correlations are built up from the initial state, determined by the relevant statistical operator $\hat{\rho}_{\rm rel}(t)$, and (A4) means that observed statistical averages $\langle\cdots^t\rangle$ at time t are correctly reproduced by $\hat{\rho}_{\rm rel}(t)$.

In LRT the response parameters $F_n(t)$ are considered to be small. This permits one to perform the expansion of the relevant $\hat{\rho}_{\rm rel}(t)$ and the irrelevant $\hat{\rho}_{\rm irrel}(t) = \hat{\rho}(t) - \hat{\rho}_{\rm rel}(t)$ statistical operators with respect to $F_n(t)$; see [19]. Together with (A4) and using the Kubo identity and partial integration of correlation functions, this gives rise to a system of equations,

$$\langle\delta\hat{B}_n\rangle = \sum_m (\hat{B}_n; \delta\hat{B}_m)F_m, \qquad \text{(A5)}$$

$$\sum_m [-i\omega\{(\hat{B}_n; B_m) + \langle\hat{\hat{B}}_m; \delta B_m\rangle_z\} + (\hat{B}_n; \hat{\hat{B}}_m) + \langle\hat{\hat{B}}_n; \hat{\hat{B}}_m\rangle_z]F_m$$
$$= \beta\frac{e}{m}\{(\hat{B}_n; \hat{\boldsymbol{P}}_1) + \langle\hat{\hat{B}}_m; \hat{\boldsymbol{P}}_1\rangle_z\}\boldsymbol{E}, \qquad \text{(A6)}$$

where $z = \omega + i\delta$; $\delta\hat{B}_n = \hat{B}_n - \langle\hat{B}_n\rangle_0$, where $\langle\hat{B}_n\rangle_0$ is the statistical average of $\hat{B}_n$ with the equilibrium density operator ρ_0.

The quantity $\hat{\boldsymbol{P}}_1 = \hat{\boldsymbol{B}}_0(0) = \hat{\boldsymbol{P}}_{0,1}$ is the operator of the total momentum of electrons given by Eq. (11) (we consider the long-wavelength limit $k \to 0$). The operators $\hat{B}_n$ are also chosen in the form of Eq. (11) (as well as $\hat{\boldsymbol{P}}_1$, they are vectors).

At the leading order of the parameter of interaction, proportional to e^2, one can show [27] that the terms containing only one operator $\hat{\hat{B}}_n$ can be omitted. For the set (11) of observables, the equilibrium averages vanish, $\langle\hat{B}_n\rangle_0 = 0$. Keeping this in mind, one can derive from (A5) and (A6) the following expressions, which determine the values of the density of electric current $\langle\hat{\boldsymbol{J}}\rangle = e\langle\hat{\boldsymbol{P}}_1\rangle$ and the response parameters F_n:

$$\boldsymbol{J} = \frac{ne^2}{m}\boldsymbol{E}\sum_m \mathfrak{N}_{1m}\mathcal{F}_m, \qquad \text{(A7)}$$
$$\sum_m [\mathfrak{C}_{nm} - i\tilde{\omega}\mathfrak{N}_{nm}]\mathcal{F}_m = \mathfrak{N}_{n1}, \qquad \text{(A8)}$$

where the dimensionless correlation functions and response parameters are defined in Eq. (20).

APPENDIX B: EVALUATION OF CORRELATION FUNCTIONS

Correlation functions introduced in Eq. (20) can be expressed as

$$\mathfrak{C}_{nm}^{\rm ei}(\omega) = iZ/(3\pi^2)\int_0^\infty f_{\rm scr}(y)dy\int_{-\infty}^\infty \frac{dx}{x}\frac{R_{nm}^{\rm ei}(x,y)}{w + i\delta - x}$$
$$\times \ln\left[\frac{1 + e^{\epsilon_\mu - (x/y - y)^2}}{1 + e^{\epsilon_\mu - (x/y + y)^2}}\right], \qquad \text{(B1)}$$

$$\mathfrak{C}_{nm}^{\rm ee}(\omega) = i/(3\sqrt{2}\pi^2)\int_0^\infty f_{\rm scr}^{\rm e}(y)dy\int_{-\infty}^\infty \frac{dx}{x}\frac{R_{nm}^{\rm ee}(x,y)}{w + i\delta - x}$$
$$\times \ln\left[\frac{1 + e^{\epsilon_\mu - (x/y - y)^2}}{1 + e^{\epsilon_\mu - (x/y + y)^2}}\right], \qquad \text{(B2)}$$

where $\mathfrak{C}_{nm}^{\rm ee}(\omega)$ and $\mathfrak{C}_{nm}^{\rm ei}(\omega)$ are the contributions owing to electron-electron and electron-ion interaction, respectively, and $\mathfrak{C}_{nm} = \mathfrak{C}_{nm}^{\rm ee} + \mathfrak{C}_{nm}^{\rm ei}$. Expressions $R_{nm}^{\rm ei}$ and $R_{nm}^{\rm ee}$ are polynomials of x and y. For $n,m = 1,3$ they have the following form (see [19]):

$$R_{11}^{\rm ei} = 1, \quad R_{31}^{\rm ei} = R_{13}^{\rm ei} = 1 + y^2 + 3x^2,$$
$$R_{33}^{\rm ei} = 2 + 2y^2 + y^4 + 2x^2(5 + 3y^2) + 9x^4,$$
$$R_{11}^{\rm ee} = R_{31}^{\rm ee} = R_{13}^{\rm ee} = 0, \quad R_{33}^{\rm ee} = 1 + 19x^2/4. \qquad \text{(B3)}$$

Similar expressions can be given for the higher order polynomials; see Refs. [36,123].

The screening function $f_{\rm scr}^{\rm e}(y)$ is defined as

$$f_{\rm scr}^{\rm e}(y) = y^3/\left[y^2 + \tilde{k}_{\rm D}^2/4\right] \qquad \text{(B4)}$$

and the screening function $f_{\rm scr}^{\rm i}(y) \equiv f_{\rm scr}(y)$ is defined above; see Eqs. (35), (39), and (41) and Eq. (64) in the case of pseudopotentials. The value of $\tilde{k}_{\rm D}$ is given by Eq. (45). Note that in (B4) $\tilde{k}_{\rm D}$ contains the numerical factor $1/4$ instead of $1/8$ in the similar expression (35).

As done above [see Eqs. (36) and (37)], the correlation functions can be decomposed into a real part and a imaginary part using the Sokhotski-Plemej formula. One obtains for the real part of the correlation functions the expression

$$\mathfrak{C}'^{eq}_{nm} = \alpha_q/(3\pi w)\int_0^\infty f_{\rm scr}^q(y)dy\,R_{nm}^{eq}\left(\frac{w}{y}, y\right)$$
$$\times \ln\left[\frac{1 + e^{\epsilon_\mu - (w/y - y)^2}}{1 + e^{\epsilon_\mu - (w/y + y)^2}}\right], \qquad \text{(B5)}$$

where $q = {\rm i}$ or e, $\alpha_{\rm i} = Z$, $\alpha_{\rm e} = 1/\sqrt{2}$.

For the imaginary part of the correlation functions one obtains

$$\mathfrak{C}''^{eq}_{nm} = \frac{\alpha_q}{3\pi^2 w}\int_0^\infty f_{\rm scr}^q(y)dy\left[\sum_{\delta=\pm1}\mathcal{I}_{nm}^{eq,\delta}(y) - 2\mathcal{I}_{nm}^{eq,0}(y)\right], \qquad \text{(B6)}$$

$$\mathcal{I}_{nm}^{eq,l} = \int_0^\infty \frac{d\xi}{\xi}\sum_{\sigma=\pm1}\sigma R_{nm}^{eq}\left(\xi + \sigma\frac{lw}{y}, y\right)$$
$$\times \ln[1 + e^{\epsilon_\mu - [\xi + \sigma(y + lw/y)]^2}], \qquad \text{(B7)}$$

with $l = 0, \pm 1$.

[1] L. Pugachev, N. Andreev, P. Levashov, Y. Malkov, A. Stepanov, and D. Yashunin, Plasma Phys. Rep. **41**, 542 (2015).

[2] N. E. Andreev, L. P. Pugachev, M. E. Povarnitsyn, and P. R. Levashov, Laser Part. Beams **34**, 115 (2016).

[3] O. F. Kostenko, N. E. Andreev, O. N. Rosmej, and A. Schoenlein, J. Phys: Confer. Ser. (2016) (to be published).

[4] O. Kostenko and N. Andreev, Quantum Electron. **43**, 237 (2013).

[5] O. F. Kostenko, Quantum Electron. **44**, 478 (2014).

[6] G. Zimmerman, D. Kershaw, D. Bailey, and J. Harte, *LASNEX Code for Inertial Confinement Fusion*, Report No. UCRL-80169, CONF-780202-9, http://www.osti.gov/scitech/servlets/purl/5207118.

[7] A. Djaoui and S. J. Rose, J. Phys. B **25**, 2745 (1992).

[8] K. Eidmann, J. Meyer-ter-Vehn, T. Schlegel, and S. Hüller, Phys. Rev. E **62**, 1202 (2000).

[9] M. E. Veysman, M. B. Agranat, N. E. Andreev, S. I. Ashitkov, V. E. Fortov, K. V. Khishchenko, O. F. Kostenko, P. R. Levashov, A. V. Ovchinnikov, and D. S. Sitnikov, J. Phys. B **41**, 125704 (2008).

[10] M. E. Povarnitsyn, N. E. Andreev, E. M. Apfelbaum, T. E. Itina, K. V. Khishchenko, O. F. Kostenko, P. R. Levashov, and M. E. Veysman, Appl. Surf. Sci. **258**, 9480 (2012).

[11] M. E. Povarnitsyn, N. E. Andreev, P. R. Levashov, K. V. Khishchenko, D. A. Kim, V. G. Novikov, and O. N. Rosmej, Laser Part. Beams **31**, 663 (2013).

[12] N. Andreev, M. Povarnitsyn, M. Veysman, A. Faenov, P. Levashov, K. V. Khishchenko, T. Pikuz, A. Magunov, O. Rosmej, A. Blazevic, A. Pelka, G. Schaumann, M. Schollmeier, and M. Roth, Laser Part. Beams **33**, 541 (2015).

[13] M. Agranat, N. Andreev, S. Ashitkov, M. Veysman, P. Levashov, A. Ovchinnikov, D. Sitnikov, V. Fortov, and K. Khishchenko, JETP Lett. **85**, 271 (2007).

[14] P. Schmuser, M. Dohlus, J. Rossbach, and C. Behrens, *Free-Electron Lasers in the Ultraviolet and X-Ray Regime. Physical Principles, Experimental Results, Technical Realization* (Springer, Berlin, 2014).

[15] J. Sekutowicz, V. Ayvazyan, M. Barlak, J. Branlard, W. Cichalewski, W. Grabowski, D. Kostin, J. Lorkiewicz, W. Merz, R. Nietubyc, R. Onken, A. Piotrowski, K. Przygoda, E. Schneidmiller, and M. Yurkov, Phys. Rev. Spec. Top.–Accel. Beams **18**, 050701 (2015).

[16] B. A. Reagan, M. Berrill, K. A. Wernsing, C. Baumgarten, M. Woolston, and J. J. Rocca, Phys. Rev. A **89**, 053820 (2014).

[17] P. Sperling, E. J. Gamboa, H. J. Lee, H. K. Chung, E. Galtier, Y. Omarbakiyeva, H. Reinholz, G. Röpke, U. Zastrau, J. Hastings, L. B. Fletcher, and S. H. Glenzer, Phys. Rev. Lett. **115**, 115001 (2015).

[18] D. N. Zubarev, V. Morozov, and G. Röpke, *Relaxation and Hydrodynamic Processes* (Akademie Verlag/Wiley, Berlin, 1997), Vol. 2.

[19] H. Reinholz and G. Röpke, Phys. Rev. E **85**, 036401 (2012).

[20] H. Reinholz, Ann. Phys. Fr. **30**, 1 (2005).

[21] G. Röpke, Phys. Rev. E **57**, 4673 (1998).

[22] H.-J. Kull and L. Plagne, Phys. Plasmas **8**, 5244 (2001).

[23] E. M. Lifshitz and L. P. Pitaevskii, *Physical Kinetics* (Butterworth-Heinemann, Oxford, U.K., 1981), p. 217.

[24] N. E. Andreev, M. E. Veysman, V. P. Efremov, and V. E. Fortov, High Temp. **41**, 594 (2003) [Teplofiz. Vys. Temp. **41** 679 (2003)].

[25] M. E. Veysman, B. Cros, N. E. Andreev, and G. Maynard, Phys. Plasmas **13**, 053114 (2006).

[26] Y. V. Arkhipov, A. B. Ashikbayeva, A. Askaruly, A. E. Davletov, and I. M. Tkachenko, Phys. Rev. E **90**, 053102 (2014).

[27] H. Reinholz, R. Redmer, G. Röpke, and A. Wierling, Phys. Rev. E **62**, 5648 (2000).

[28] H. Reinholz, G. Röpke, S. Rosmej, and R. Redmer, Phys. Rev. E **91**, 043105 (2015).

[29] D. V. Knyazev and P. R. Levashov, Phys. Plasmas **21**, 073302 (2014).

[30] G. Norman, I. Saitov, V. Stegailov, and P. Zhilyaev, Contrib. Plasma Phys. **53**, 300 (2013).

[31] P. A. Zhilyaev, G. E. Norman, I. M. Saitov, and V. V. Stegailov, Phys. Dokl. **58**, 277 (2013).

[32] H. Reinholz, I. Morozov, G. Röpke, and T. Millat, Phys. Rev. E **69**, 066412 (2004).

[33] I. Morozov, H. Reinholz, G. Röpke, A. Wierling, and G. Zwicknagel, Phys. Rev. E **71**, 066408 (2005).

[34] W. A. Stygar, G. A. Gerdin, and D. L. Fehl, Phys. Rev. E **66**, 046417 (2002).

[35] S. Skupsky, Phys. Rev. A **36**, 5701 (1987).

[36] V. S. Karakhtanov, R. Redmer, H. Reinholz, and G. Ropke, Contrib. Plasma Phys. **53**, 639 (2013).

[37] A. Alexandrov, L. Bogdankevich, and A. Rukhadze, *Principles of Plasma Electrodynamics* (Springer Verlag, Heidelberg, 1984).

[38] D. Pines and P. Nozieres, *The Theory of Quantum Liquids* (Westview Press, Boulder, CO, 1999).

[39] V. D. Gorobchenko and E. G. Maksimov, Sov. Phys. Usp. **23**, 35 (1980).

[40] G. Röpke, R. Redmer, A. Wierling, and H. Reinholz, Phys. Rev. E **60**, R2484 (1999).

[41] G. Röpke and A. Wierling, Phys. Rev. E **57**, 7075 (1998).

[42] For longer laser pulses the plasma expansion can lead to an increase of L_∇ up to length of plasma inhomogeneity or the laser wavelength.

[43] G. Röpke, Phys. Rev. A **38**, 3001 (1988).

[44] N. R. Arista and W. Brandt, Phys. Rev. A **29**, 1471 (1984).

[45] Note that in the case of statical screening $f_{\rm scr}$ is dependent only on y, rather than on y and w; see (42) and (43) and discussion below these formulas.

[46] D. O. Gericke, J. Vorberger, K. Wünsch, and G. Gregori, Phys. Rev. E **81**, 065401 (2010).

[47] G. Faussurier, C. Blancard, P. Combis, and L. Videau, Phys. Plasmas **21**, 092706 (2014).

[48] W. Johnson, C. Guet, and G. Bertsch, J. Quant. Spectrosc. Radiat. Transfer **99**, 327 (2006).

[49] M. Y. Kuchiev and W. R. Johnson, Phys. Rev. E **78**, 026401 (2008).

[50] Note that the derivation of the inverse bremsstrahlung at high frequencies based on considering the emission of an electron scattered at a Coulomb center, as conducted in [51,52], gives rise to a $\nu_{\rm eff} \sim \omega^{-2/3}$ dependence of the effective collision frequency on the laser frequency, instead of a $\sim\omega^{-3/2}$ dependence as it follows from our consideration; see (50). The reason of this discrepancy is presently not clear.

[51] V. Krainov, J. Exp. Theor. Phys. **92**, 960 (2001).

[52] V. P. Krainov, J. Phys. B **33**, 1585 (2000).

[53] L. Schlessinger and J. Wright, Phys. Rev. A **20**, 1934 (1979).

[54] A. Wierling, T. Millat, G. Ropke, R. Redmer, and H. Reinholz, Phys. Plasmas **8**, 3810 (2001).

[55] C. Fortmann, H. Reinholz, G. Ropke, and A. Wierling, arXiv:physics/0502051.

[56] C. Fortmann, H. Reinholz, G. Röpke, and A. Wierling, *Condensed Matter Theories* (Nova Science, New York, 2005), Vol. 20.

[57] G. Bekefi, *Radiation Processes in Plasmas* (Wiley, New York, 1966).

[58] H. A. Kramers, Philos. Mag. **46**, 836 (1923).

[59] A. Sommerfeld, *Atombau und Spektrallinien* (Vieweg-Verlag, Braunschweig, 1949).

[60] H. Totsuji, Phys. Rev. A **32**, 3005 (1985).

[61] V. B. Berestetskii, L. P. Pitaevskii, and E. Lifshitz, *Quantum Electrodynamics: Course of Theoretical Physics* (Elsevier, Burlington, 2008), Vol. 4.

[62] R. Kawakami, K. Mima, H. Totsuji, and Y. Yokoyama, Phys. Rev. A **38**, 3618 (1988).

[63] A. Höll, V. G. Morozov, and G. Röpke, Phys. A (Amsterdam, Neth.) **319**, 371 (2003).

[64] F. J. Blatt, *Theory of Mobility of Electrons in Solids*, Solid State Physics, Vol. 4, edited by F. Seitz and D. Turnbull (Academic Press, New York, 1957), pp. 199–366.

[65] P. Thakor, Y. Sonvane, and A. Jani, Phys. Chem. Liq. **49**, 530 (2011).

[66] J.-L. Bretonnet and A. Derouiche, Phys. Rev. B **38**, 9255 (1988).

[67] N. W. Ashcroft and D. Stroud, *Theory of the Thermodynamics of Simple Liquid Metals*, Solid State Physics, Vol. 33, edited by H. Ehrenreich, F. Seitz, and D. Turnbull (Academic Press, New York, 1978), pp. 1–81.

[68] H. B. Nersisyan, M. E. Veysman, N. E. Andreev, and H. H. Matevosyan, Phys. Rev. E **89**, 033102 (2014).

[69] A. V. Brantov, V. Y. Bychenkov, and W. Rozmus, J. Exp. Theor. Phys. **106**, 983 (2008).

[70] A. Esser, R. Redmer, and G. Röpke, Contrib. Plasma Phys. **43**, 33 (2003).

[71] Y. T. Lee and R. M. More, Phys. Fluids **27**, 1273 (1984).

[72] S. E. Kirkwood, Y. Y. Tsui, R. Fedosejevs, A. V. Brantov, and V. Y. Bychenkov, Phys. Rev. B **79**, 144120 (2009).

[73] M. Basko, T. Löwer, V. N. Kondrashov, A. Kendl, R. Sigel, and J. Meyer-ter-Vehn, Phys. Rev. E **56**, 1019 (1997).

[74] A. Selchow, G. Röpke, and K. Morawetz, Nucl. Instrum. Methods Phys. Res., Sect. A **441**, 40 (2000).

[75] O. F. Kostenko and N. E. Andreev, GSI Annual Report No. GSI-2008-2, 2008, p. 44.

[76] M. E. Veysman and N. E. Andreev, J. Phys. Conf. Ser. **653**, 012004 (2015).

[77] A. V. Lugovskoy and I. Bray, Phys. Rev. B **60**, 3279 (1999).

[78] D. F. Price, R. M. More, R. S. Walling, G. Guethlein, R. L. Shepherd, R. E. Stewart, and W. E. White, Phys. Rev. Lett. **75**, 252 (1995).

[79] The degeneracy was not accounted for in the original work [35].

[80] I. T. Yakubov, Phys. Usp. **36**, 365 (1993).

[81] J. Dawson and C. Oberman, Phys. Fluids **5**, 517 (1962).

[82] C. D. Decker, W. B. Mori, J. M. Dawson, and T. Katsouleas, Phys. Plasmas **1**, 4043 (1994).

[83] J. R. Adams, N. S. Shilkin, V. E. Fortov, V. K. Gryaznov, V. B. Mintsev, R. Redmer, H. Reinholz, and G. Röpke, Phys. Plasmas **14**, 062303 (2007).

[84] V. Fortov, I. Iakubov, and A. Khrapak, *Physics of Strongly Coupled Plasma* (Oxford University Press, Oxford, U.K., 2006).

[85] Initially, in [34], nondegenerate plasmas are considered; the generalization to degenerate plasmas is formally introduced by means of appropriate expression for v_*.

[86] F. J. Rogers, Phys. Rev. A **23**, 1008 (1981).

[87] Here we consider the case of low-intensity energy fluxes I_L, when one can disregard nonlinear effects in the dependence of the permittivity (or the effective collision frequency) on the electric-field strength [22,82,88]. For high enough laser pulse intensities the plasma can be heated to temperatures higher than several hundred eV. In this case, and for short laser pulses, when formation of a plasma corona is not pronounced, spacial dispersion of the permittivity can be essential [89], which restricts the present collisional approach. Besides that, we neglect modifications of plasma properties by the probe laser pulse. If this is not justified, one should average the local absorption coefficient over time and space to obtain experimentally measured values $\bar{A} = \iint I_L(\boldsymbol{r},t)A(\boldsymbol{r},t)d^3\boldsymbol{r}dt / \iint I_L(\boldsymbol{r},t)d^3\boldsymbol{r}dt$.

[88] A. B. Langdon, Phys. Rev. Lett. **44**, 575 (1980).

[89] R. Cauble and W. Rozmus, Phys. Rev. E **52**, 2974 (1995).

[90] V. P. Silin and A. A. Rukhadze, *Electromagnetic Properties of Plasma and Plasma-like Media*, 3rd ed. (URSS, Moscow, 2013) [in Russian].

[91] Strictly speaking, a quasistationary thermal ionization state of solid-density aluminum plasma with $Z = 3$ corresponds to temperatures $T \leqslant 30$ eV [24]. At higher temperatures larger values of Z may occur. In addition, in the case of ultrafast heating during times $t \ll 10$ fs strong nonequilibrium may arise so that an equilibrium result for the ionization degree Z is not justified to use. In order not to overload physical considerations, we neglect the dependence of Z on T and treat Z as constant, equal to 3 for aluminum.

[92] Y. Ivanov, V. Mintsev, V. Fortov, and A. Dremin, Sov. Phys. JETP **74**, 112 (1976).

[93] N. Shilkin, S. Dudin, V. Gryaznov, V. Mintsev, and V. Fortov, J. Exp. Theor. Phys. **97**, 922 (2003).

[94] Y. Zaporoghets, V. Mintsev, V. Gryaznov, V. Fortov, H. Reinholz, T. Raitza, and G. Röpke, J. Phys. A **39**, 4329 (2006).

[95] V. Gryaznov, I. Iosilevskiy, V. Fortov, A. Starostin, V. Roerich, V. A. Baturin, and S. V. Ayukov, Contrib. Plasma Phys. **53**, 392 (2013).

[96] H. Reinholz, G. Röpke, I. Morozov, V. Mintsev, Y. Zaparoghets, V. Fortov, and A. Wierling, J. Phys. A **36**, 5991 (2003).

[97] H. Reinholz, Y. Zaporoghets, V. Mintsev, V. Fortov, I. Morozov, and G. Röpke, Phys. Rev. E **68**, 036403 (2003).

[98] T. Raitza, H. Reinholz, G. Röpke, V. Mintsev, and A. Wierling, J. Phys. A **39**, 4393 (2006).

[99] M. Winkel, H. Reinholz, A. Wierling, G. Röpke, Y. Zaporozhets, and V. Mintsev, Contrib. Plasma Phys. **49**, 687 (2009).

[100] G. Norman, I. Saitov, V. Stegailov, and P. Zhilyaev, Phys. Rev. E **91**, 023105 (2015).

[101] Y. B. Zeldovich and Y. P. Raizer, *Physics of Shock Waves and High-Temperature Hydrodynamic Phenomena* (Academic Press, New York, 1966–1967).
[102] E. V. Stupochenko, PMTF (Prikl. Mekh. Tekh. Fiz.) **19**, 116 (1965) [in Russian].
[103] L. Landau and E. Lifshitz, *Hydrodynamics* (Nauka, Moscow, 1986).
[104] T. G. Elizarova, I. A. Shirokov, and S. Montero, Phys. Fluids **17**, 068101 (2005).
[105] K. B. Jordan, Direct numeric simulation of shock wave structures without the use of artificial viscosity, Dissertation, Marquette University, 2011.
[106] X. Qian and Z. T. Deng, Int. J. Mod. Eng. **11**, 74 (2010).
[107] V. I. Kolobov and R. R. Arslanbekov, J. Comput. Phys. **231**, 839 (2012).
[108] A. Phelps, C. Greene, and J. Burke, J. Phys. B **33**, 2965 (2000).
[109] M. Veysman, Dissertation, JIHT RAS, Moscow, 2001 [in Russian].
[110] A. V. Lankin, G. E. Norman, and I. M. Saitov, *XXX International Conference on Interaction of Intense Energy Fluxes with Matter*, Book of Abstracts (2015), http://www.ihed.ras.ru/elbrus15/abstracts/book_of_abstracts_2015_v2+titul_web.pdf.
[111] W. Kraeft, D. Kremp, W. Ebeleing, and G. Röpke, *Quantum Statistics of Charged Particle Systems* (Akademie Verlag, Berlin, 1986).
[112] M. P. Desjarlais, J. D. Kress, and L. A. Collins, Phys. Rev. E **66**, 025401 (2002).
[113] A. R. Forouhi and I. Bloomer, Phys. Rev. B **34**, 7018 (1986).
[114] L. Benfatto, E. Cappelluti, L. Ortenzi, and L. Boeri, Phys. Rev. B **83**, 224514 (2011).
[115] A. D. Rakić, Appl. Opt. **34**, 4755 (1995).
[116] A. Vial, T. Laroche, M. Dridi, and L. Le Cunff, Appl. Phys. A **103**, 849 (2011).
[117] P. G. Etchegoin, E. C. Le Ru, and M. Meyer, J. Chem. Phys. **125**, 164705 (2006).
[118] A. S. Davydov, *Quantum Mechanics* (Pergamon Press, Oxford, U.K., 1965).
[119] L. L. Moseley and T. Lukes, Am. J. Phys. **46**, 676 (1978).
[120] A. Lankin and G. Norman, Contrib. Plasma Phys. **49**, 723 (2009).
[121] A. V. Lankin and G. E. Norman, J. Phys. A **42**, 214032 (2009).
[122] This value gives the best agreement of experimental results and calculations for all wavelengths considered here.
[123] R. Redmer, Phys. Rep. **282**, 35 (1997).